EUV, Soft and Hard X-Ray Optics and Beamlines

David Attwood
University of California, Berkeley

Cheiron School
September 2015
SPring-8

The short wavelength region of the electromagnetic spectrum

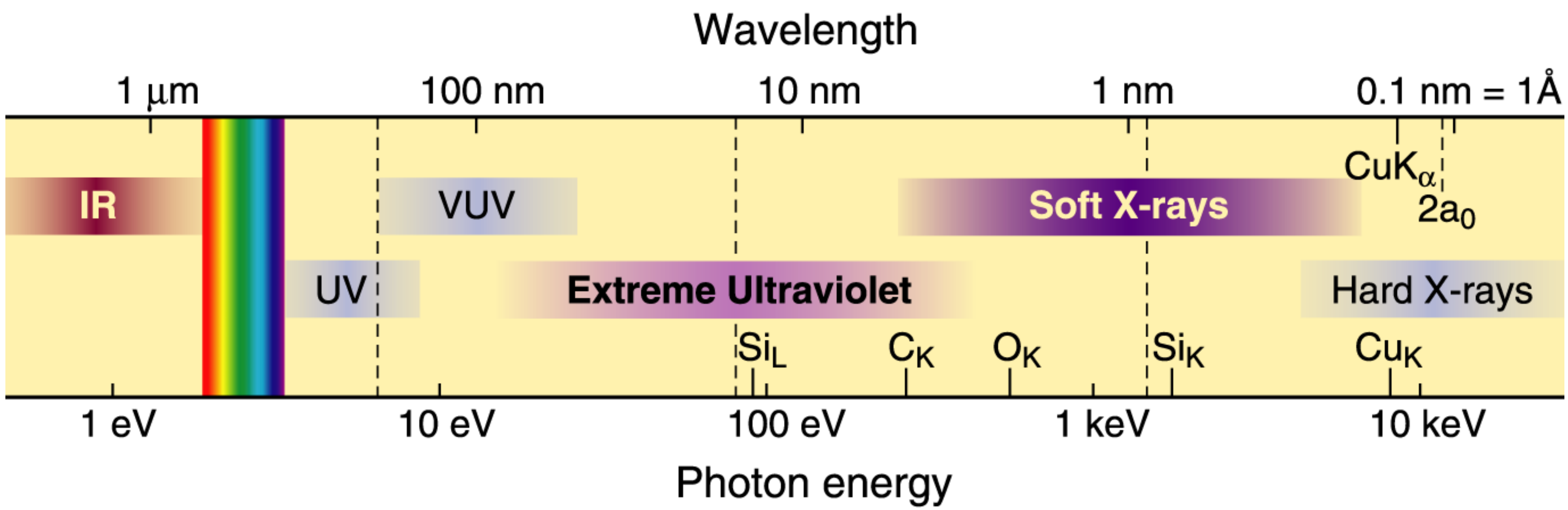

- **See smaller features**
- **Write smaller patterns**
- **Elemental and chemical sensitivity**

$$\hbar\omega \cdot \lambda = hc = 1239.842 \text{ eV nm}$$

$$n = 1 - \delta + i\beta \qquad \delta, \beta << 1$$

Available x-ray optical techniques

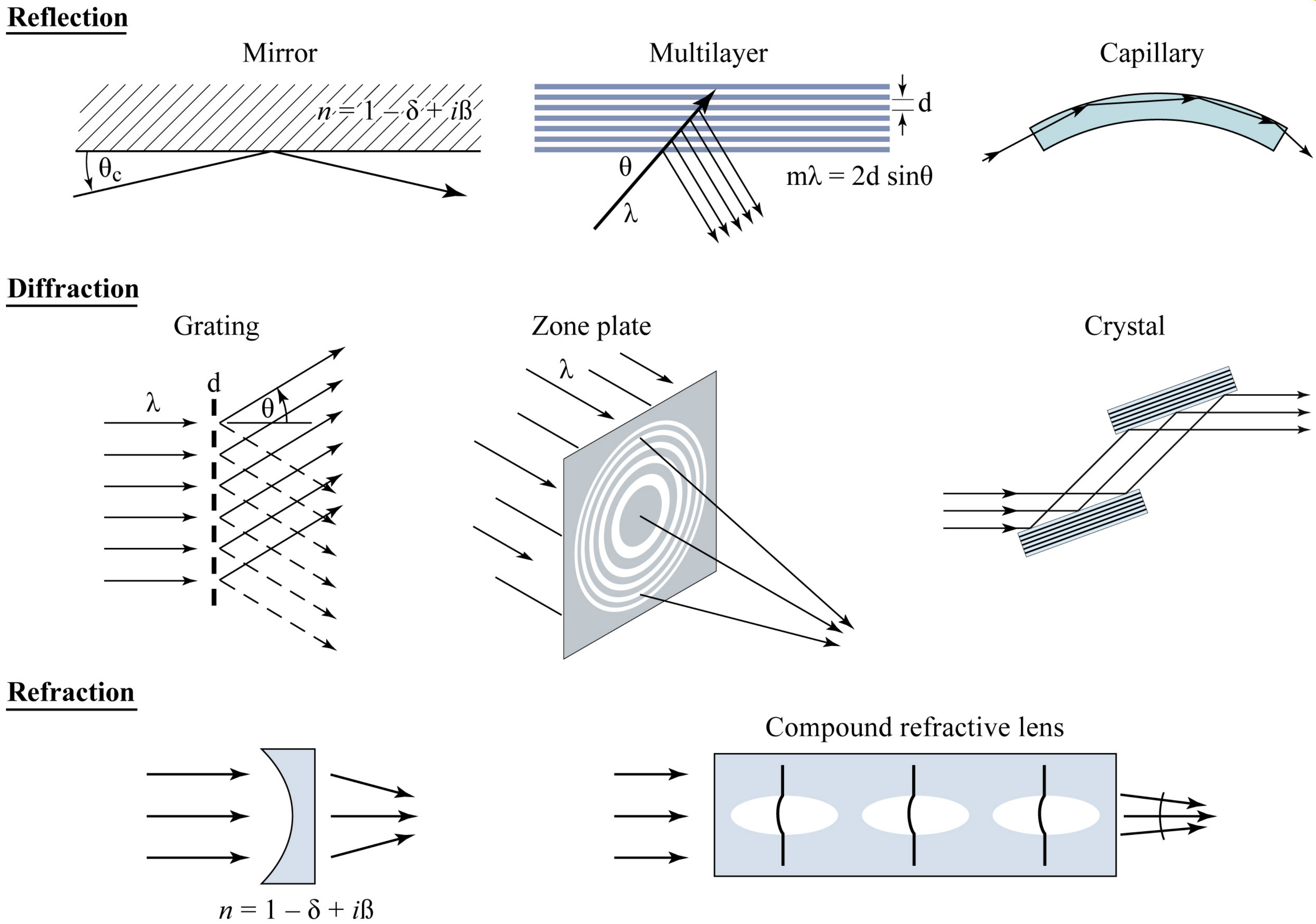

Ch 10 F0 CUP II rgb.ai

Beamlines are used to transport photons to the sample, and take a desired spectral slice

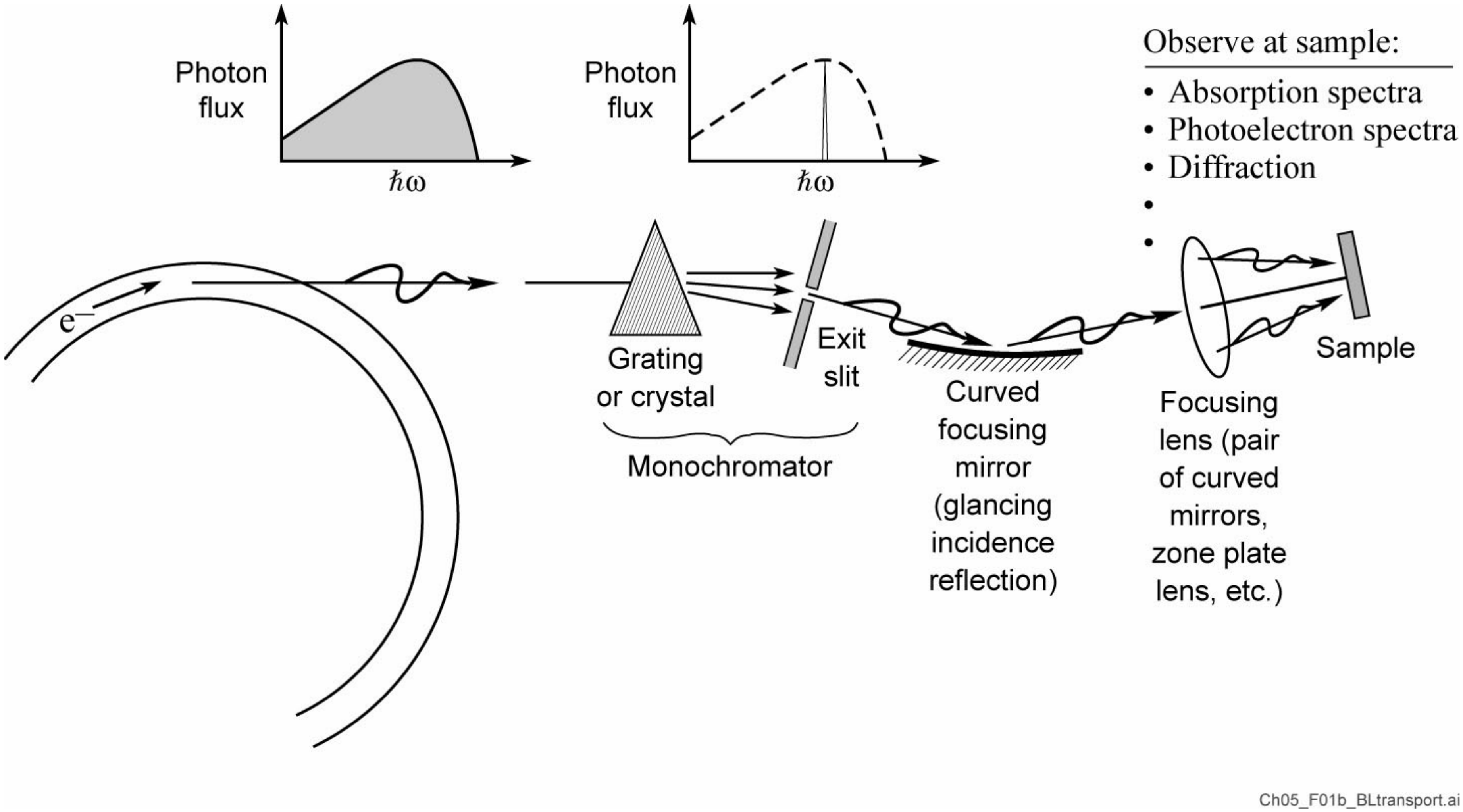

A typical beamline: monochromator plus focusing optics to deliver radiation to the sample

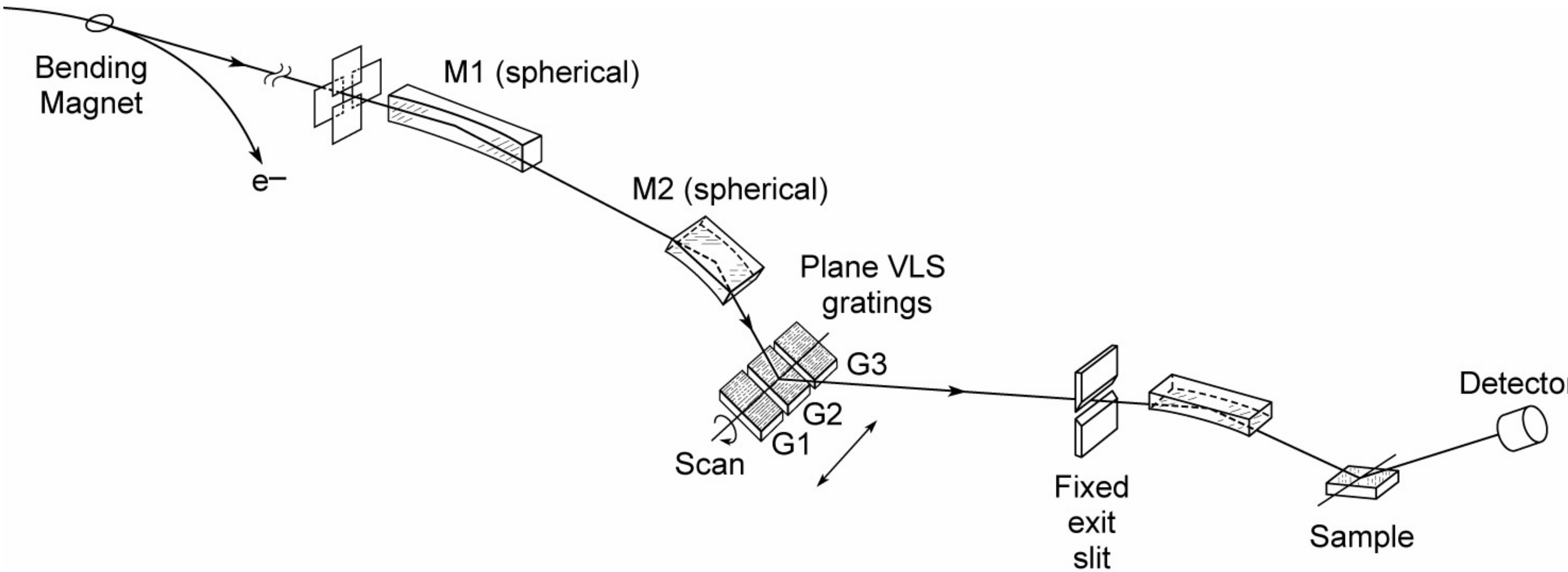

Courtesy of James Underwood (EUV Technology Inc.)

XBD9509-04496_Jan04.ai

High spectral resolution (meV beamline)

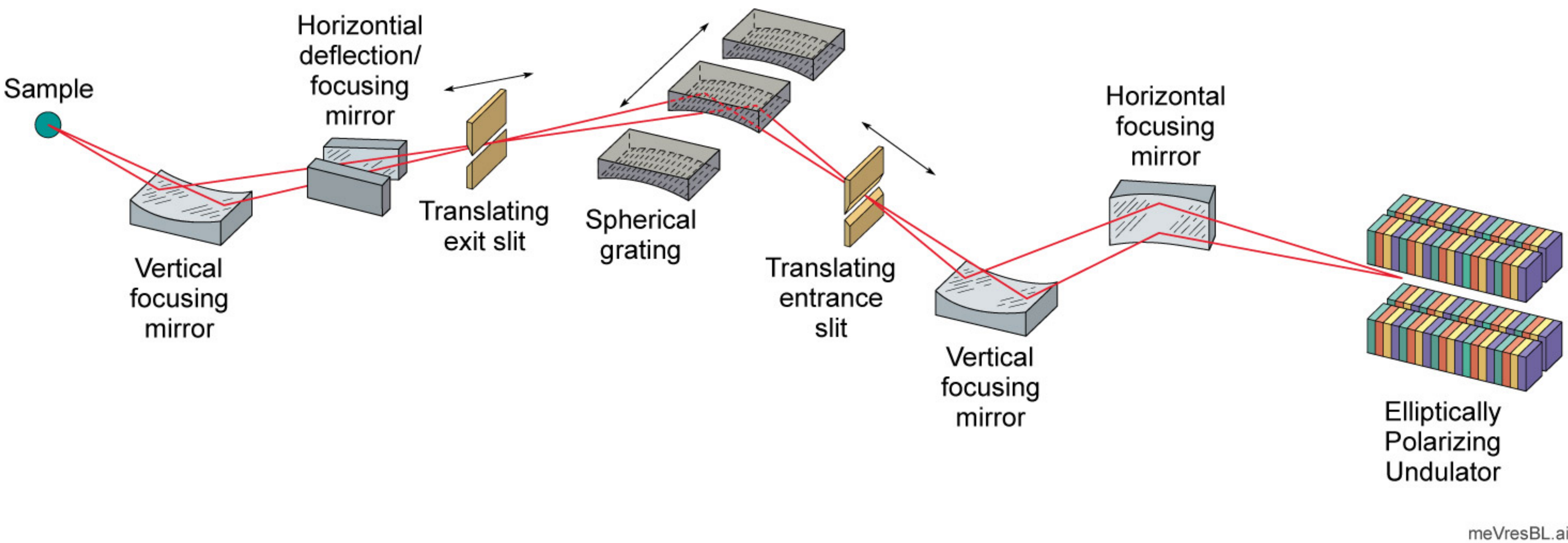

Courtesy of Zahid Hussein (ALS)

Beamline 7.0 at Berkeley's Advanced Light Source

Basic ionization and emission processes in isolated atoms

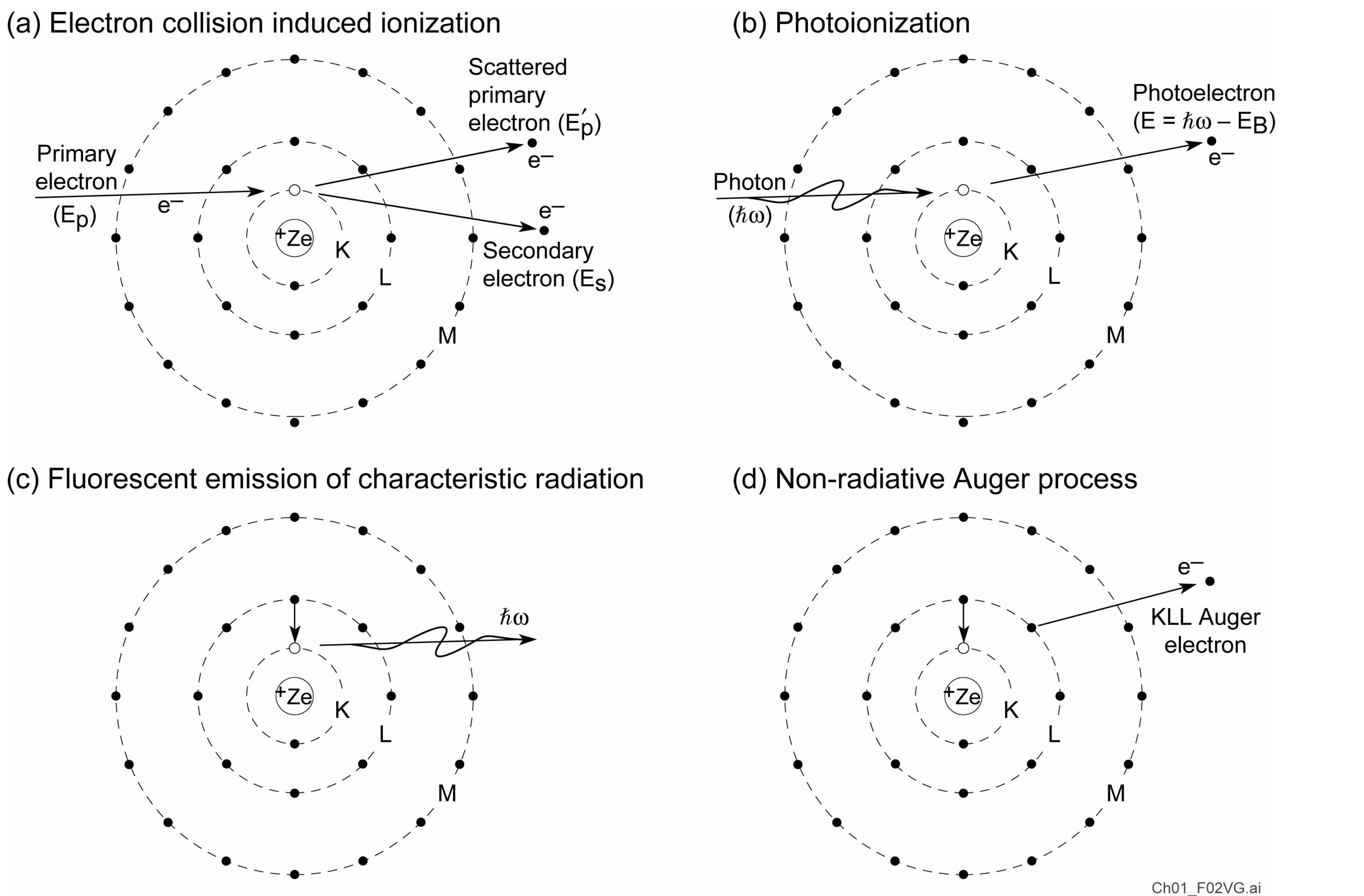

Energy levels, absorption edges, and characteristic line emissions for a multi-electron atom

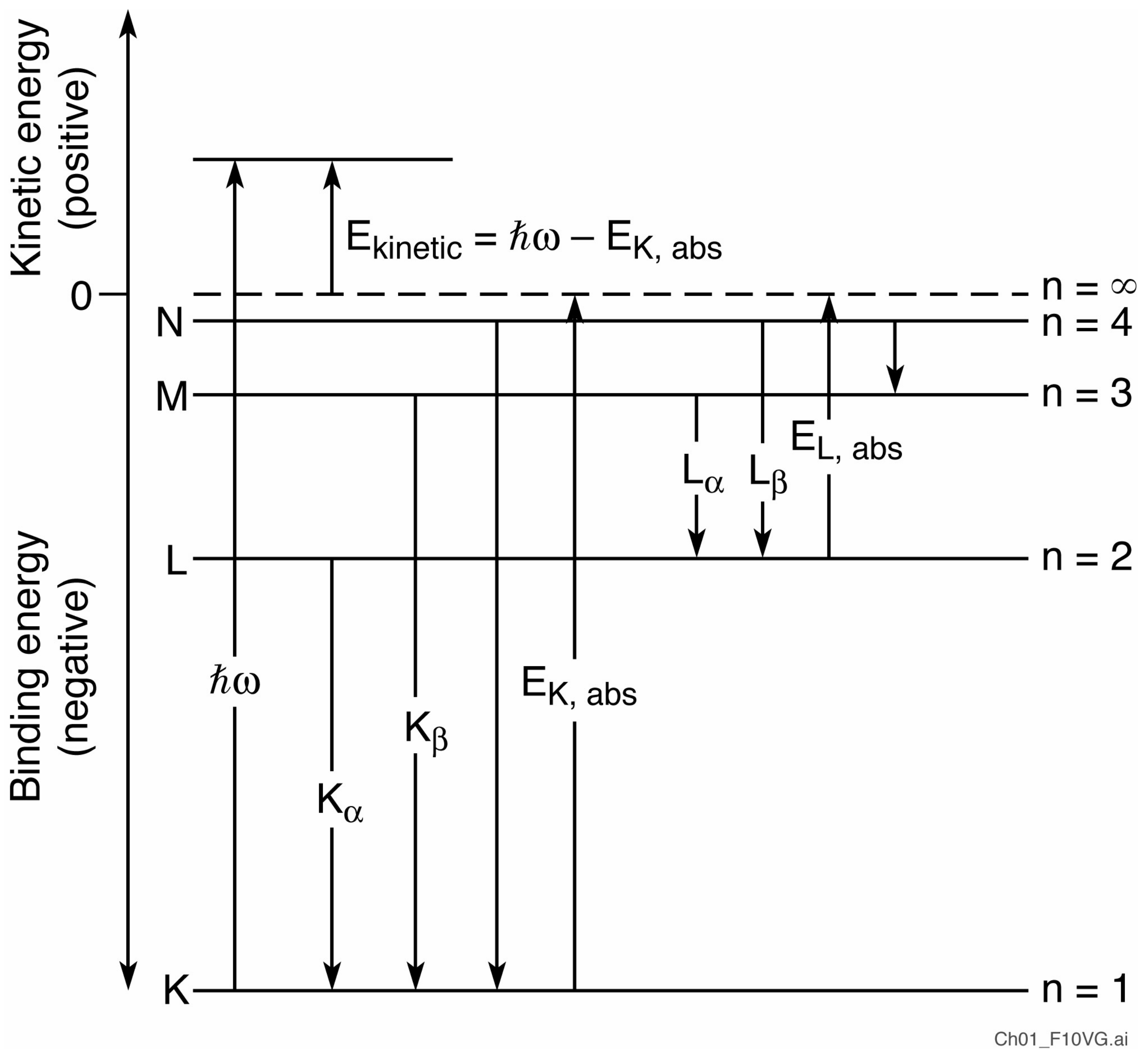

Energy levels, quantum numbers, and allowed transitions for the copper atom

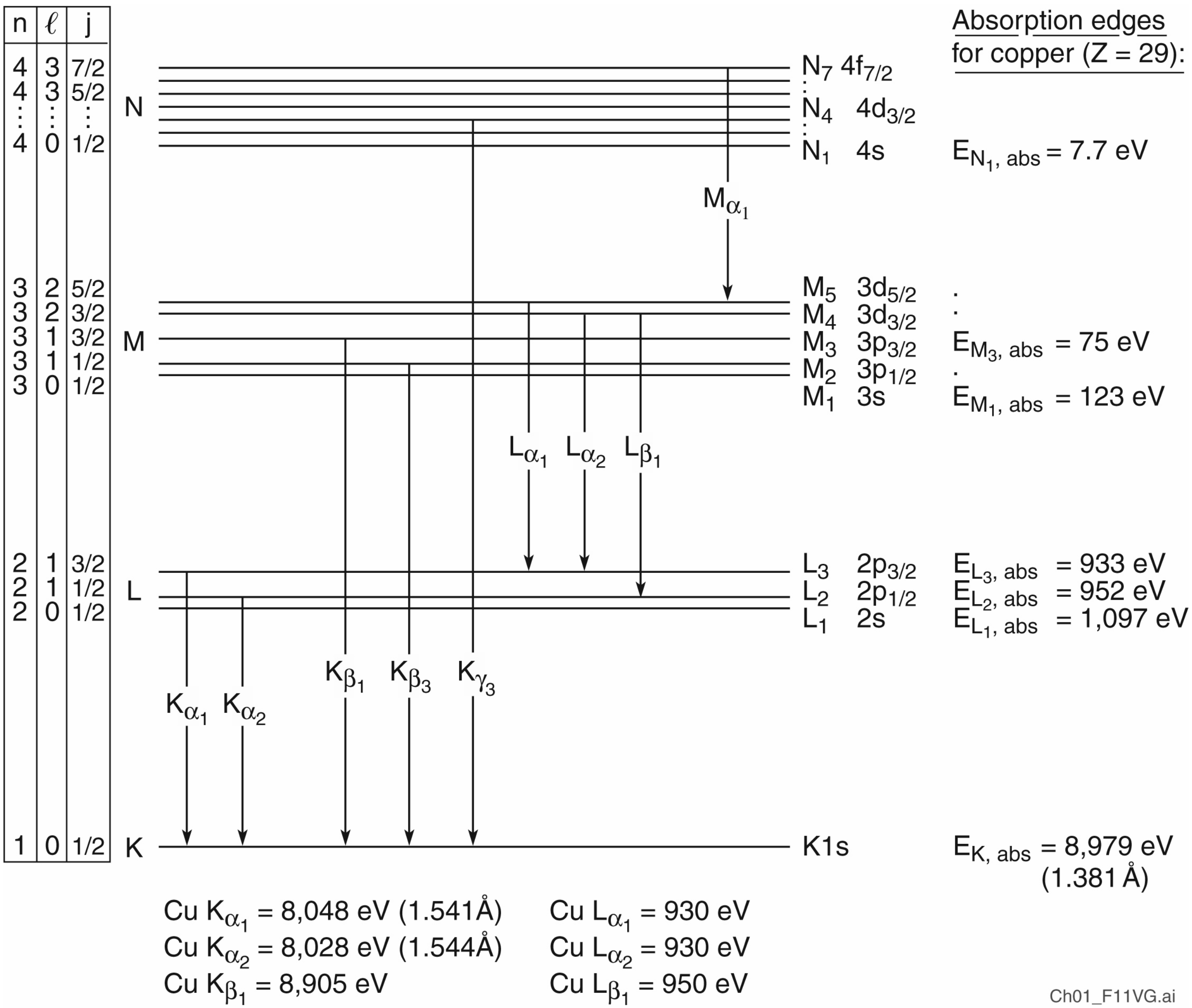

Refractive index from the IR to x-ray spectral region

$$\boxed{n(\omega) = 1 - \delta + i\beta} \quad (3.12)$$

$$\delta = \frac{n_a r_e \lambda^2}{2\pi} f_1^0(\omega) \quad (3.13a)$$

$$\beta = \frac{n_a r_e \lambda^2}{2\pi} f_2^0(\omega) \quad (3.13b)$$

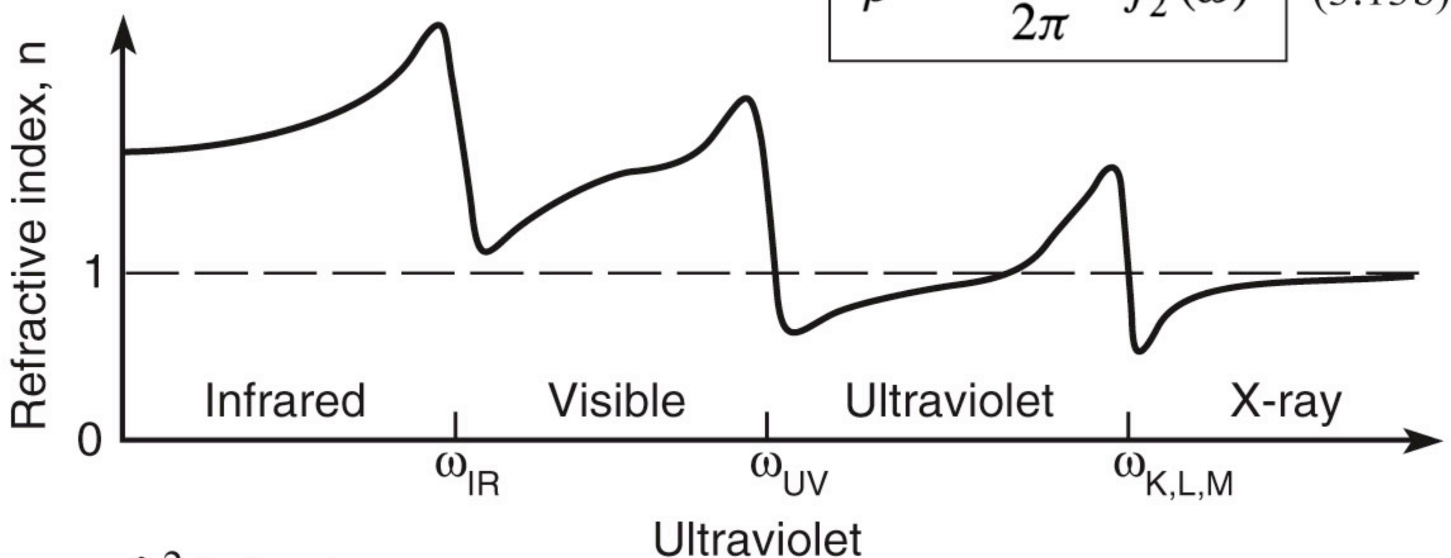

- λ^2 behavior
- δ & β << 1
- δ-crossover

Ch03_RefrcIndxIR.XR.ai

Refractive index at nanometer wavelengths

Refractive Index

$$n = 1 - \delta + i\beta = 1 - \frac{n_a r_e \lambda^2}{2\pi}\left(f_1^0 - i f_2^0\right)$$

Atomic scattering factors

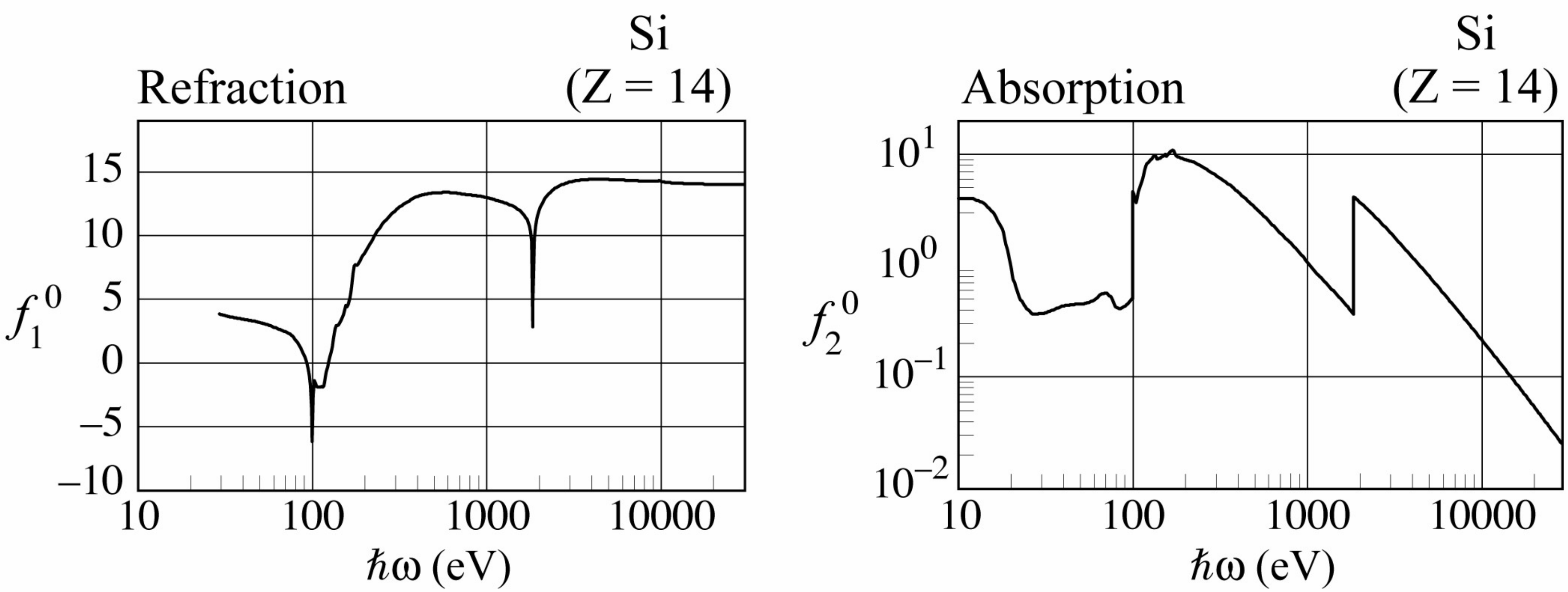

ScattrngRefracIndex_June2009.ai

Refractive index in the soft x-ray and EUV spectral region

$$n(\omega) = 1 - \frac{1}{2}\frac{e^2 n_a}{\epsilon_0 m}\sum_s \frac{g_s}{(\omega^2 - \omega_s^2) + i\gamma\omega} \qquad (3.8)$$

Noting that

$$r_e = \frac{e^2}{4\pi\epsilon_0 mc^2}$$

and that for forward scattering

$$f^0(\omega) = \sum_s \frac{g_s\omega^2}{\omega^2 - \omega_s^2 + i\gamma\omega}$$

where this has complex components

$$f^0(\omega) = f_1^0(\omega) - i f_2^0(\omega)$$

The refractive index can then be written as

$$\boxed{n(\omega) = 1 - \frac{n_a r_e \lambda^2}{2\pi}\left[f_1^0(\omega) - i f_2^0(\omega)\right]} \qquad (3.9)$$

which we write in the simplified form

$$\boxed{n(\omega) = 1 - \delta + i\beta} \qquad (3.12)$$

Ch03_RefracIndex2.ai

Photoionization and electron binding energies

TABLE B.1. Electron binding energies in electron volts for the elements in their natural forms.[a]

Element	K 1s	L_1 2s	L_2 $2p_{1/2}$	L_3 $2p_{3/2}$	M_1 3s	M_2 $3p_{1/2}$	M_3 $3p_{3/2}$	M_4 $3d_{3/2}$	M_5 $3d_{5/2}$	N_1 4s	N_2 $4p_{1/2}$	N_3 $4p_{3/2}$
1 H	13.6											
2 He	24.6[b]											
3 Li	54.7[b]											
4 Be	111.5[b]											
5 B	188[b]											
6 C	284.2[b]											
7 N	409.9[b]	37.3[b]										
8 O	543.1[b]	41.6[b]										
9 F	696.7[b]											
10 Ne	870.2[b]	48.5[b]	21.7[b]	21.6[b]								
11 Na	1070.8[c]	63.5[c]	30.4[c]	30.5[b]								
12 Mg	1303.0[c]	88.6[b]	49.6[c]	49.2[c]								
13 Al	1559.6	117.8[b]	72.9[b]	72.5[b]								
14 Si	1838.9	149.7[b]	99.8[b]	99.2[b]								
15 P	2145.5	189[b]	136[b]	135[b]								
16 S	2472	230.9[b]	163.6[b]	162.5[b]								
17 Cl	2822.4	270.2[b]	202[b]	200[b]								
18 Ar	3205.9[b]	326.3[b]	250.6[b]	248.4[b]	29.3[b]	15.9[b]	15.7[b]					
19 K	3608.4[b]	378.6[b]	297.3[b]	294.6[b]	34.8[b]	18.3[b]	18.3[b]					
20 Ca	4038.5[b]	438.4[c]	349.7[c]	346.2[c]	44.3[c]	25.4[c]	25.4[c]					
21 Sc	4492.8	498.0[b]	403.6[b]	398.7[b]	51.1[b]	28.3[b]	28.3[b]					
22 Ti	4966.4	560.9[c]	461.2[c]	453.8[c]	58.7[c]	32.6[c]	32.6[c]					
23 V	5465.1	626.7[c]	519.8[c]	512.1[c]	66.3[c]	37.2[c]	37.2[c]					
24 Cr	5989.2	695.7[c]	583.8[c]	574.1[c]	74.1[c]	42.2[c]	42.2[c]					
25 Mn	6539.0	769.1[c]	649.9[c]	638.7[c]	82.3[c]	47.2[c]	47.2[c]					
26 Fe	7112.0	844.6[c]	719.9[c]	706.8[c]	91.3[c]	52.7[c]	52.7[c]					
27 Co	7708.9	925.1[c]	793.3[c]	778.1[c]	101.0[c]	58.9[c]	58.9[c]					
28 Ni	8332.8	1008.6[c]	870.0[c]	852.7[c]	110.8[c]	68.0[c]	66.2[c]					
29 Cu	8978.9	1096.7[c]	952.3[c]	932.5[c]	122.5[c]	77.3[c]	75.1[c]					
30 Zn	9658.6	1196.2[b]	1044.9[b]	1021.8[b]	139.8[b]	91.4[b]	88.6[b]	10.2[b]	10.1[b]			

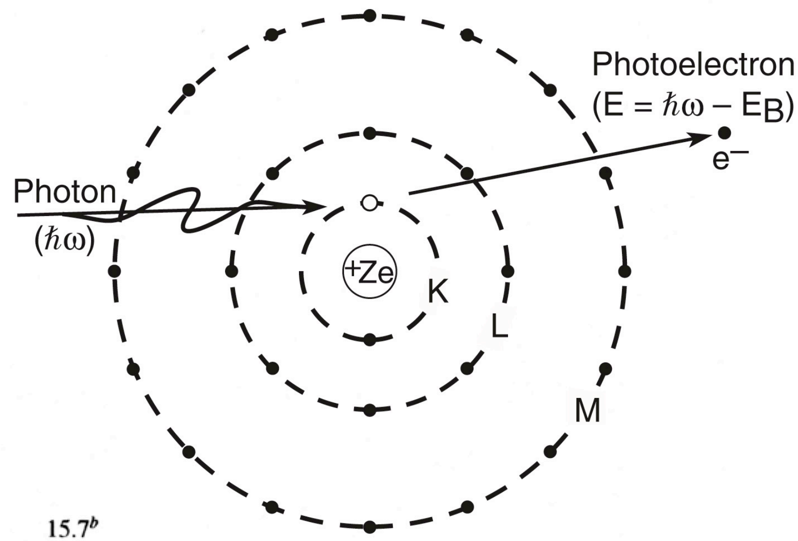

Ch01_ApB_T1rev2
& Photoionization.ai

Normal incidence reflection at an interface

$$R_s = \frac{\left|\cos\phi - \sqrt{n^2 - \sin^2\phi}\right|^2}{\left|\cos\phi + \sqrt{n^2 - \sin^2\phi}\right|^2} \tag{3.49}$$

at $\phi = 0$:

$$R_{s,\perp} = \frac{|1-n|^2}{|1+n|^2} = \frac{(1-n)(1-n^*)}{(1+n)(1+n^*)}$$

For $n = 1 - \delta + i\beta$

$$R_{s,\perp} = \frac{(\delta - i\beta)(\delta + i\beta)}{(2-\delta+i\beta)(2-\delta-i\beta)} = \frac{\delta^2+\beta^2}{(2-\delta)^2+\beta^2}$$

Reflectivity for x-ray and EUV radiation at normal incidence ($\phi = 0$):

$$\boxed{R_{s,\perp} \simeq \frac{\delta^2+\beta^2}{4}} \tag{3.50}$$

Example: Nickel @ 300 eV (4.13 nm)

$$\left.\begin{array}{ll} f_1^\circ = 17.8 & f_2^\circ = 7.70 \\ \delta = 0.0124 & \beta = 0.00538 \end{array}\right\} R_\perp = 4.58 \times 10^{-5}$$

Ch03_NormIncidReflc_5.05.ai

Hard x-ray imaging based on glancing incidence reflective optics

- Optics behave differently at these very short wavelengths (nanometers rather than 520 nm green light)
- The refractive index is less than unity, $n = 1 - \delta + i\beta$
- Waves bend away form the normal at an interface
- Absorption is significant in all materials and at all wavelength.
- Because of absorption, refractive lenses do not work, prisms do not, windows need to be extremely thin (100 nm or less).
- Because light is bent away from the surface normal, it possible to have "total external reflection" at glancing incidence – a commonly used technique.
- Kirkpatrick-Baez (KB) mirror pair

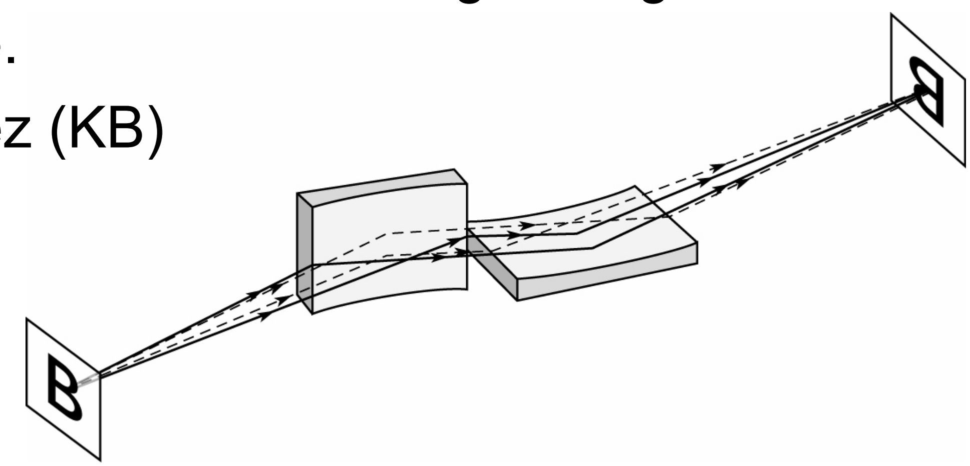

Glancing incidence optics

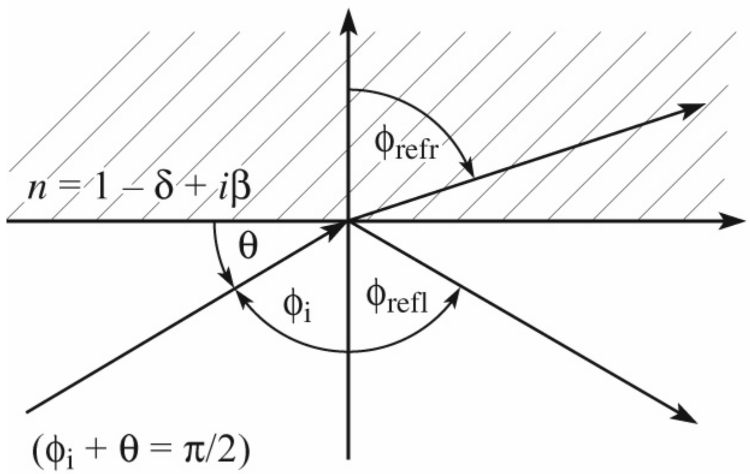

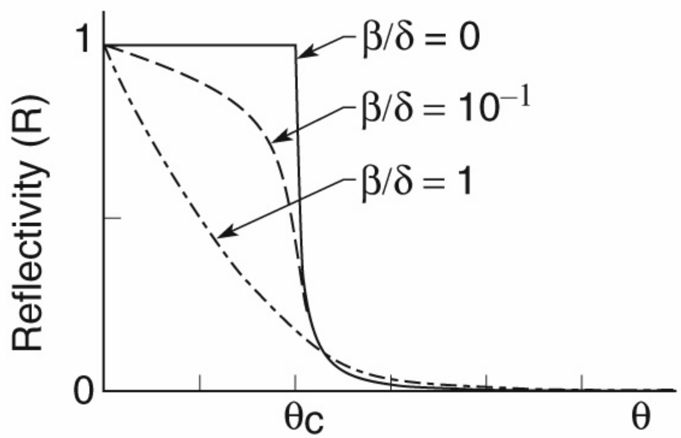

Snell's Law: $\boxed{\text{Sin } \phi_{refr.} = \frac{\text{Sin } \phi_i}{n}}$

Total external Reflection:

$$\phi_{refr.} \rightarrow \frac{\pi}{2} \text{ as } \phi_i \rightarrow \phi_{critical}$$

$$\text{Snell's Law: } 1 = \frac{\text{Sin } \phi_c}{1 - \delta}$$

$$\text{Sin}(90° - \theta_c) = 1 - \delta$$

$$\text{Cos } \theta_c = 1 - \delta$$

$$1 - \frac{\theta_c{}^2}{2} = 1 - \delta$$

$$\boxed{\theta_c = \sqrt{2\delta}}$$

For gold at 1 keV

$$\delta = 2.1 \times 10^{-3}$$

$$\theta_c = 3.7°$$

(www.cxro.LBL.gov ;
"X-ray properties of the elements"
"X-ray interaction with matter")

GlancngIncidncOptics.ai

Total external reflection with finite β

Glancing incidence reflection
as a function of β/δ

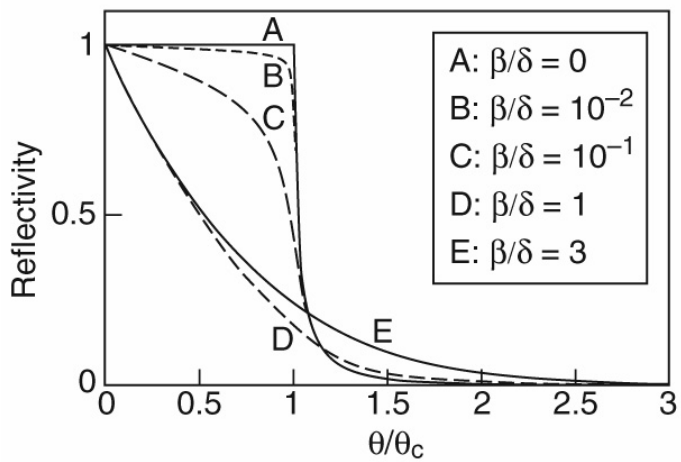

- finite β/δ rounds the sharp angular dependence
- cutoff angle and absorption edges can enhance the sharpness
- note the effects of oxide layers and surface contamination

. . . for real materials

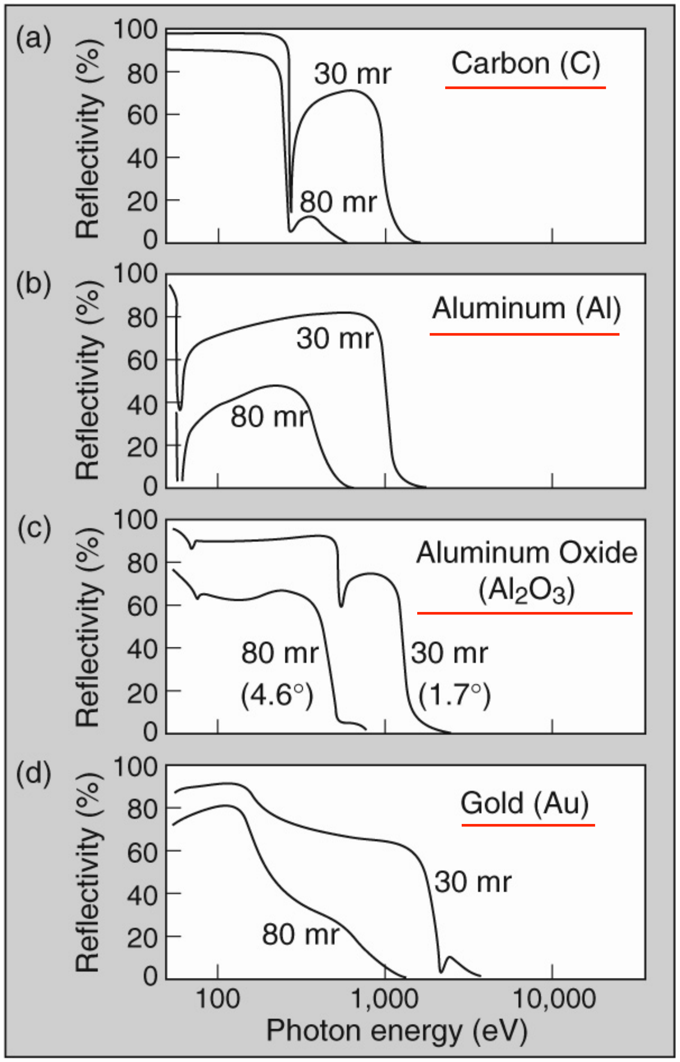

(Henke, Gullikson, Davis)

Ch03_TotalExtrnlReflc3.ai

X-ray mirrors at Glancing incidence

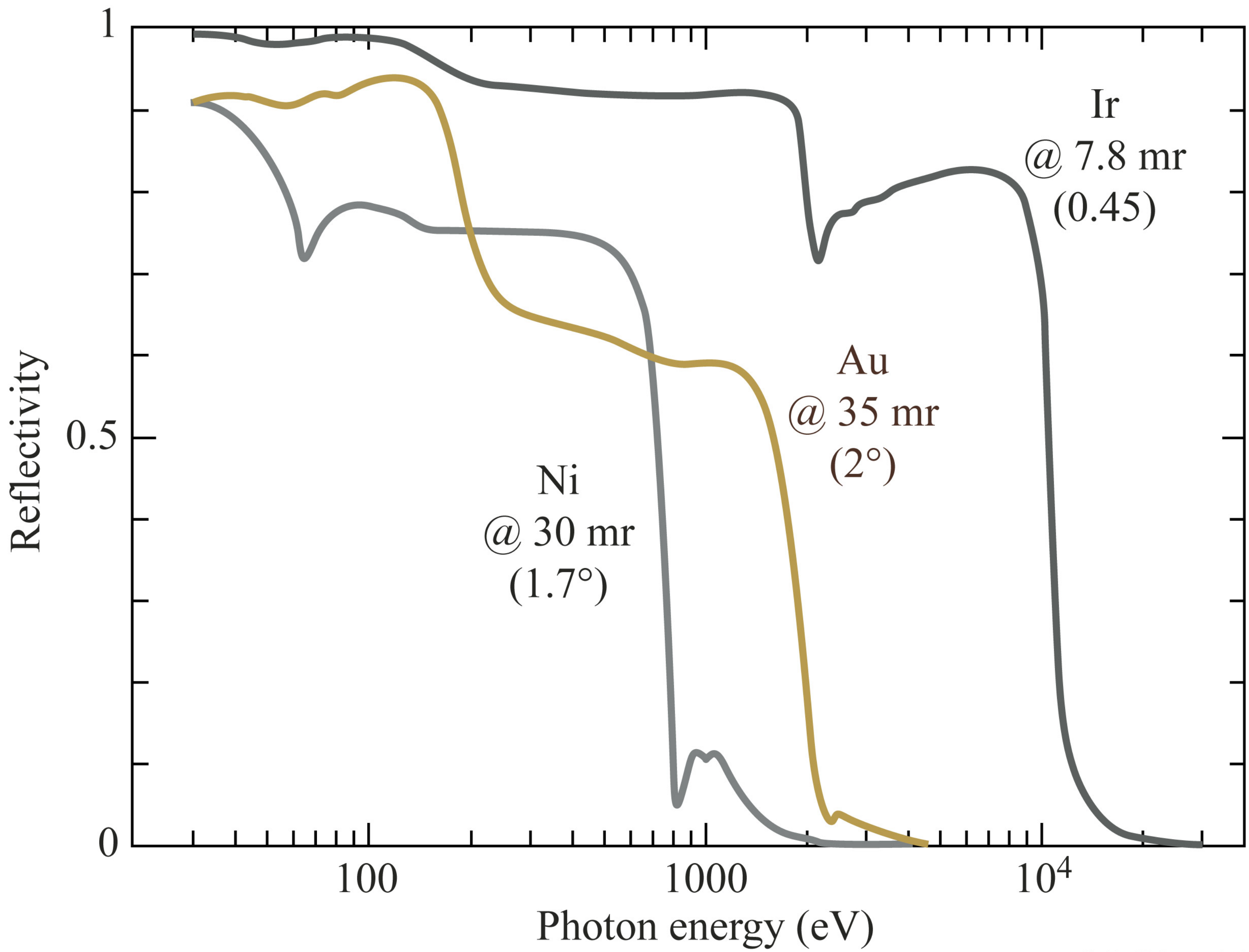

Ch 10 F02 CUP II rgb.ai

Elliptical x-ray mirrors

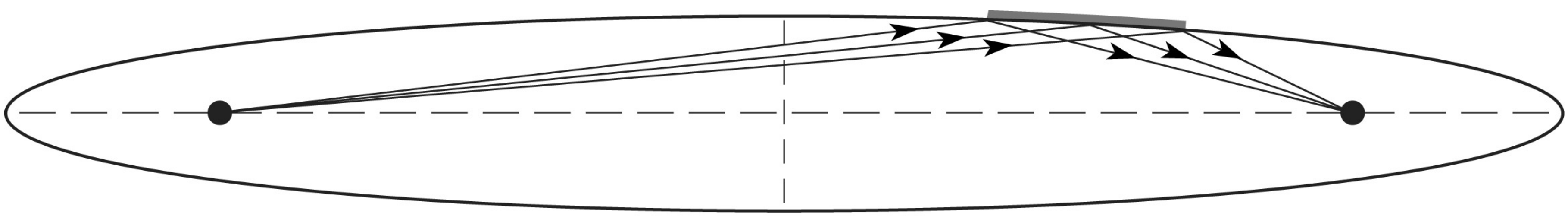

Focusing with curved glancing incidence optics

The Kirkpatrick-Baez mirror system

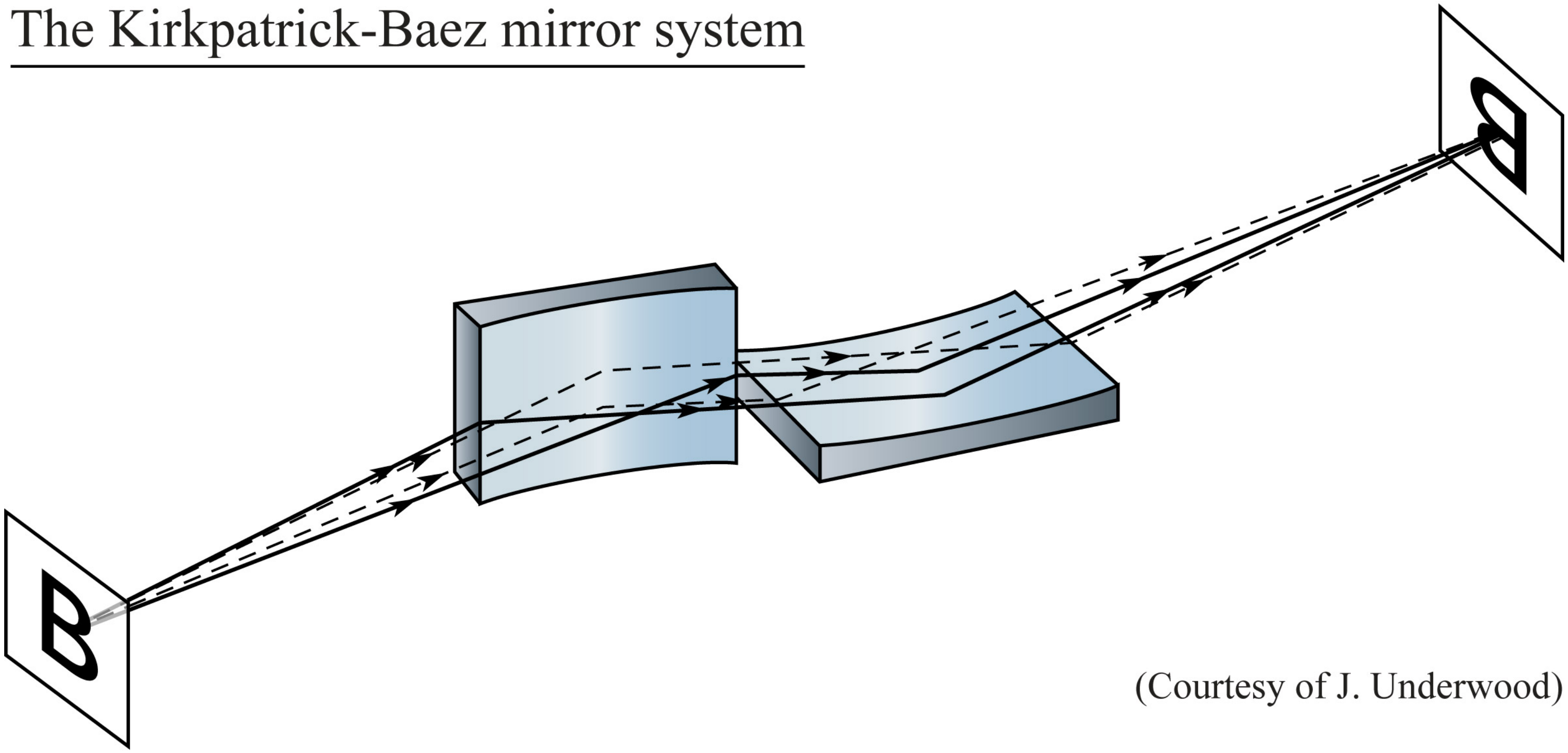

(Courtesy of J. Underwood)

- Two crossed ellipses
- Astigmatism cancels
- Common use in synchrotron radiation beamlines
- Hard x-ray nanoprobe

Ch 10 F01a CUP II rgb.ai

Glancing incidence mirrors for Astrophysics: the "spiral galaxy"

30 M light years

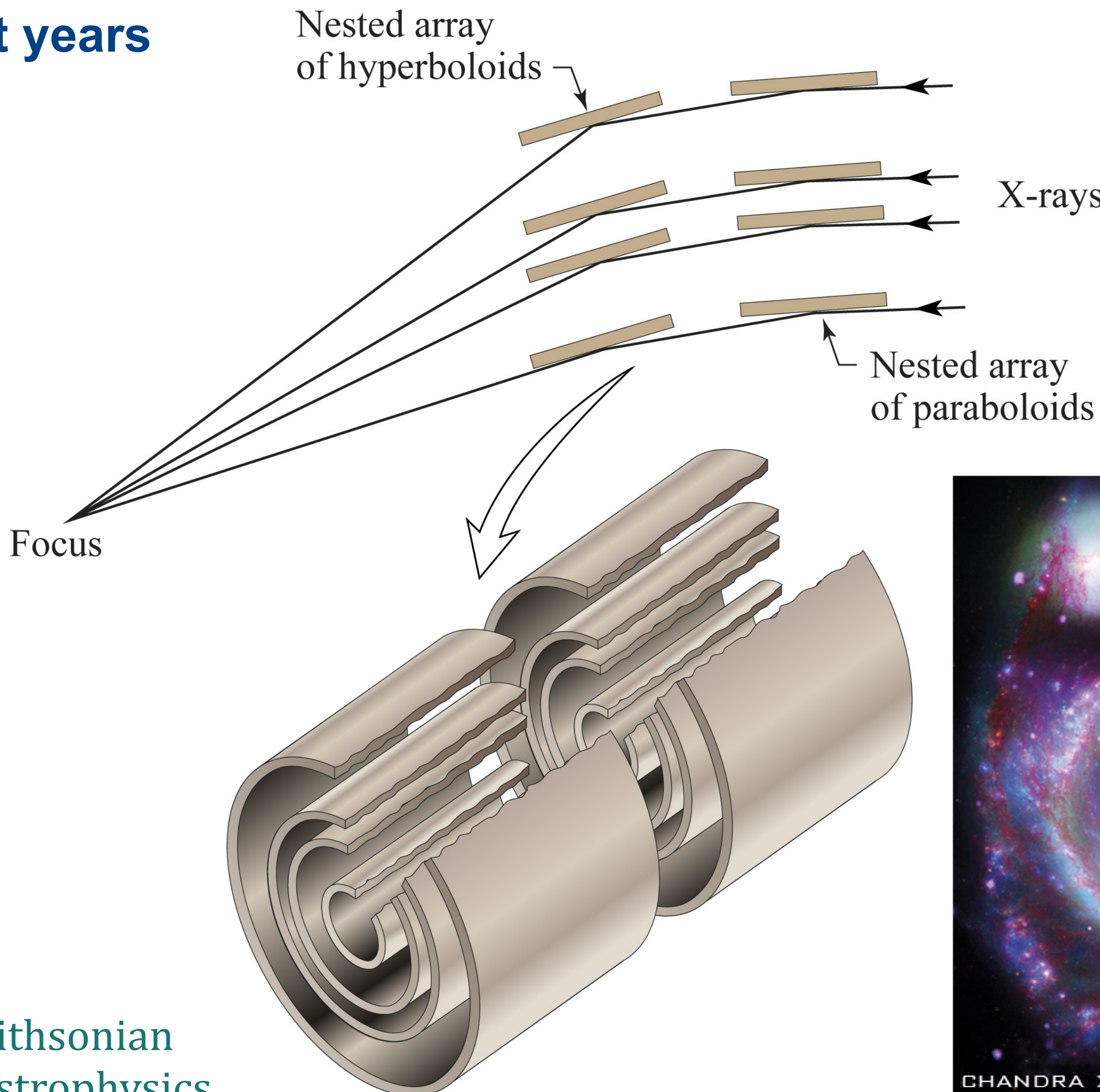

Ch 10 F04 CUP II rgb.ai

Courtesy of
Harvard-Smithsonian
Center for Astrophysics

Fluorescent microprobe based in crossed cylinders

Kirkpatrick-Baez (KB) optics

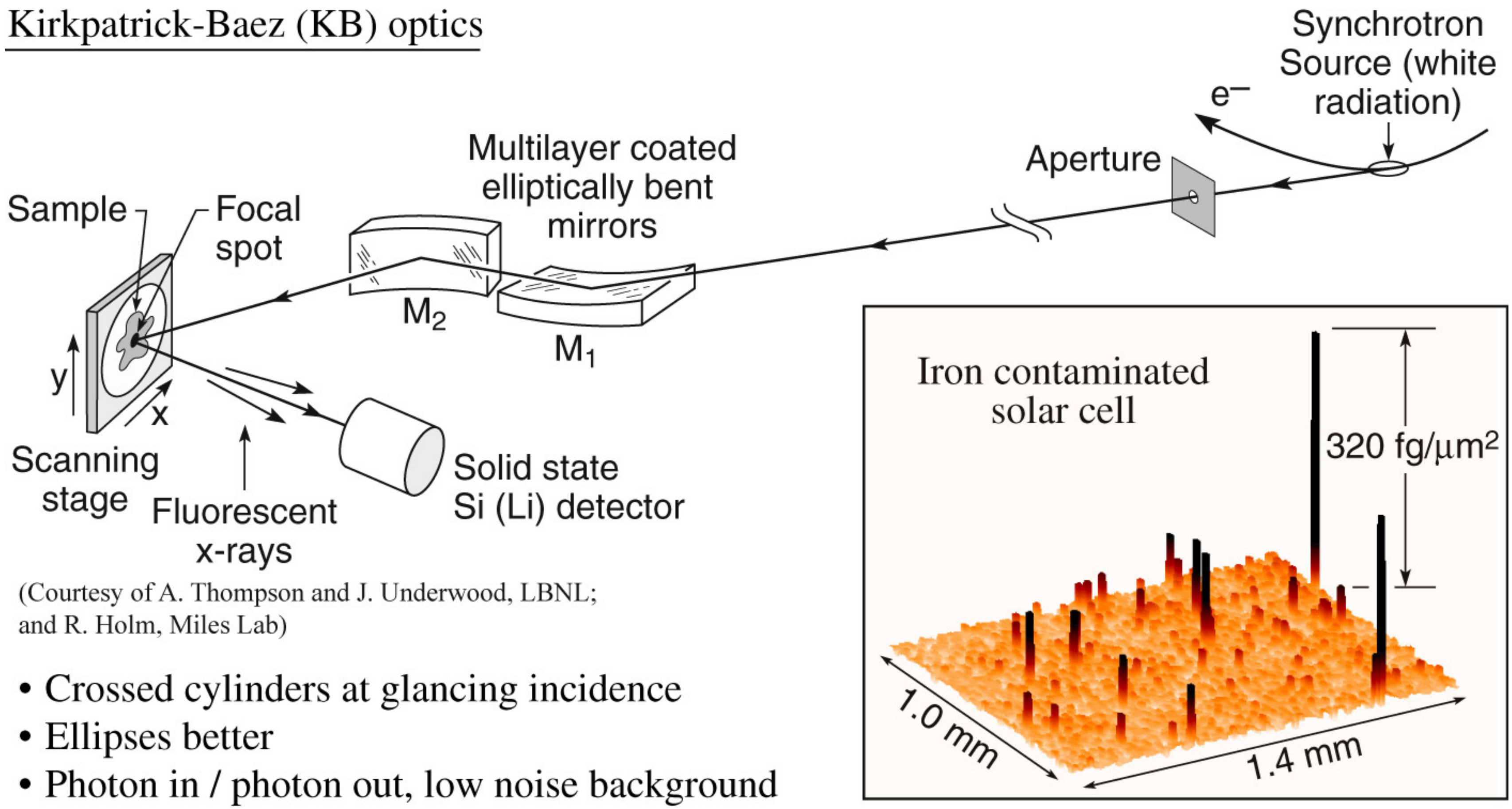

(Courtesy of A. Thompson and J. Underwood, LBNL; and R. Holm, Miles Lab)

- Crossed cylinders at glancing incidence
- Ellipses better
- Photon in / photon out, low noise background
- Femtogram and part per billion (ppb) sensitivity
- Sub-micron focus (to 0.1 µm recently), but scattering gives several micron "50% encircled energy"
- K-B optics have many applications to synchrotron beamlines, fusion diagnostics, etc.

FluoresMicroprobe.ai

Hard x-ray nanoprobe at SPring-8

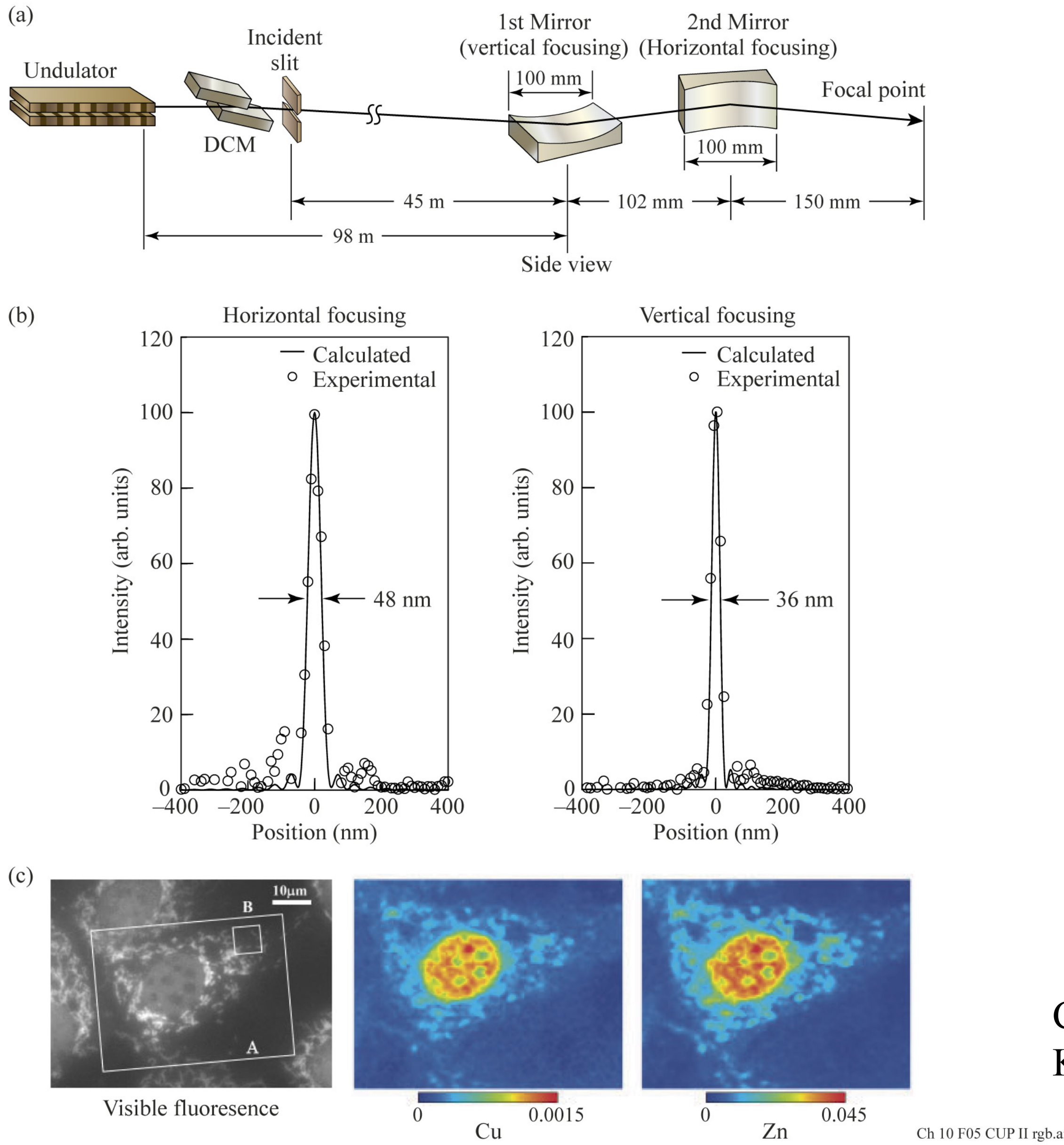

Courtesy of H. Matsuyama and K. Yamauchi, Osaka University.

Spring-8 hard x-ray nanoprobe to 7 nm spot size

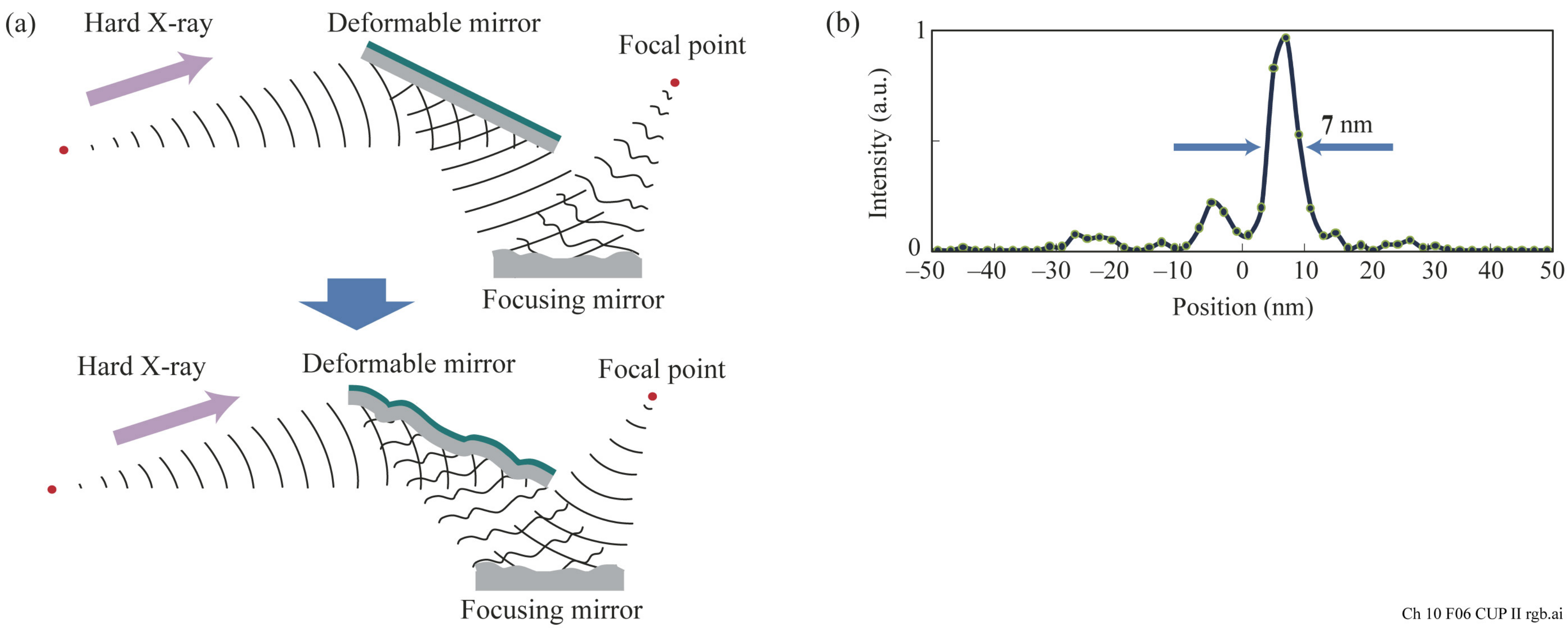

Courtesy of H. Mimura and
K. Yamauchi, Osaka University.

Diffractive optics for soft x-rays and EUV

Zone Plates **Gratings** **Pinholes**

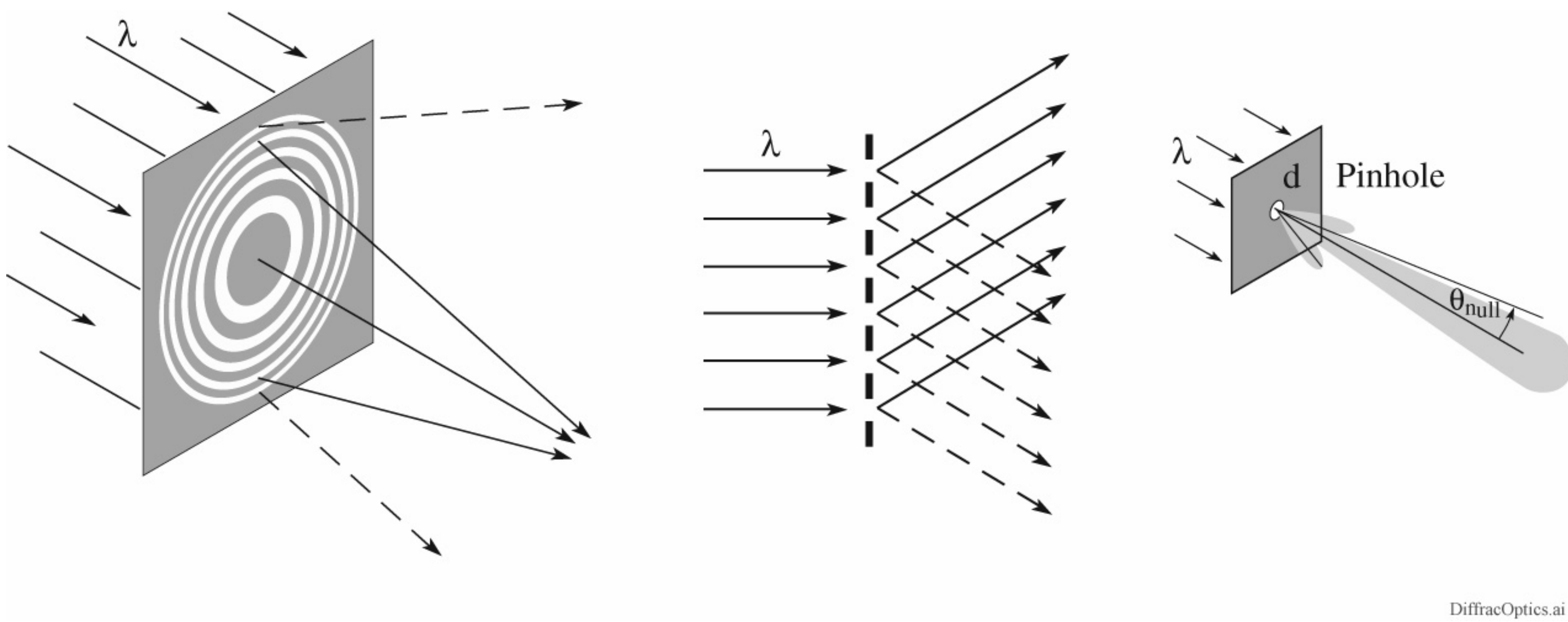

Diffraction from a transmission grating

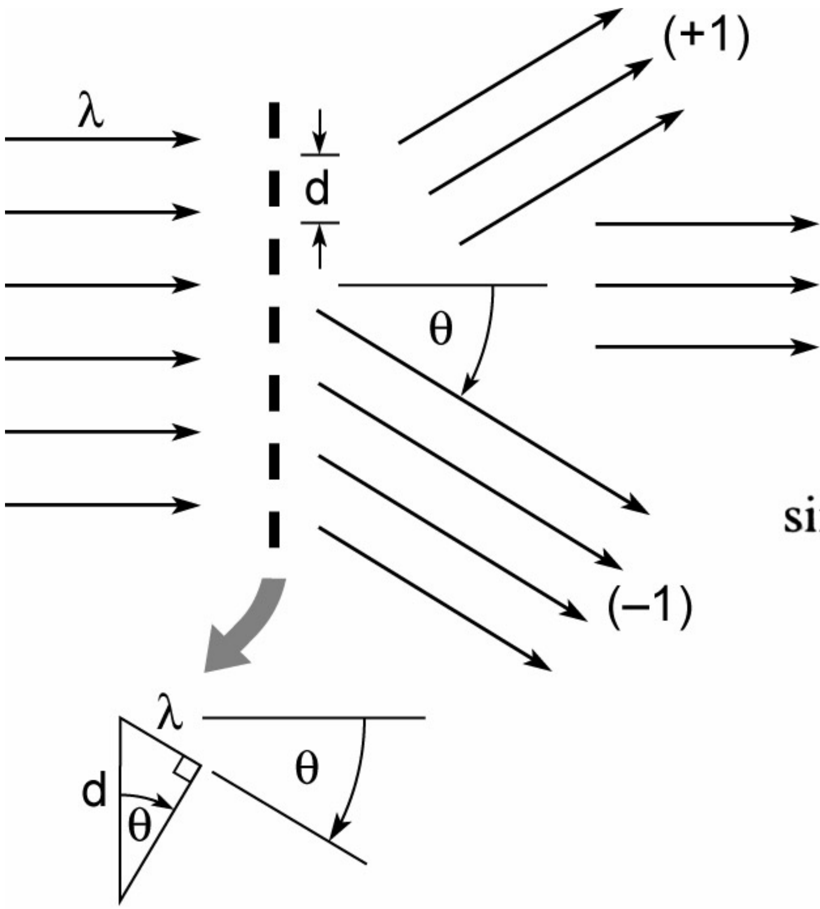

$$\sin\theta_m = \frac{m\lambda}{d}\;; \quad m = 0,\ \pm 1,\ \pm 2,\ \pm 3,\ \ldots \qquad (9.2)$$

$$\eta_m = \begin{cases} \frac{1}{4} & m = 0 \\ 1/m^2\pi^2 & m \text{ odd} \\ 0 & m \text{ even} \end{cases} \qquad (9.24)$$

(50% absorbed)

Ch09_F03VGrev.4.04.ai

A Fresnel zone plate lens

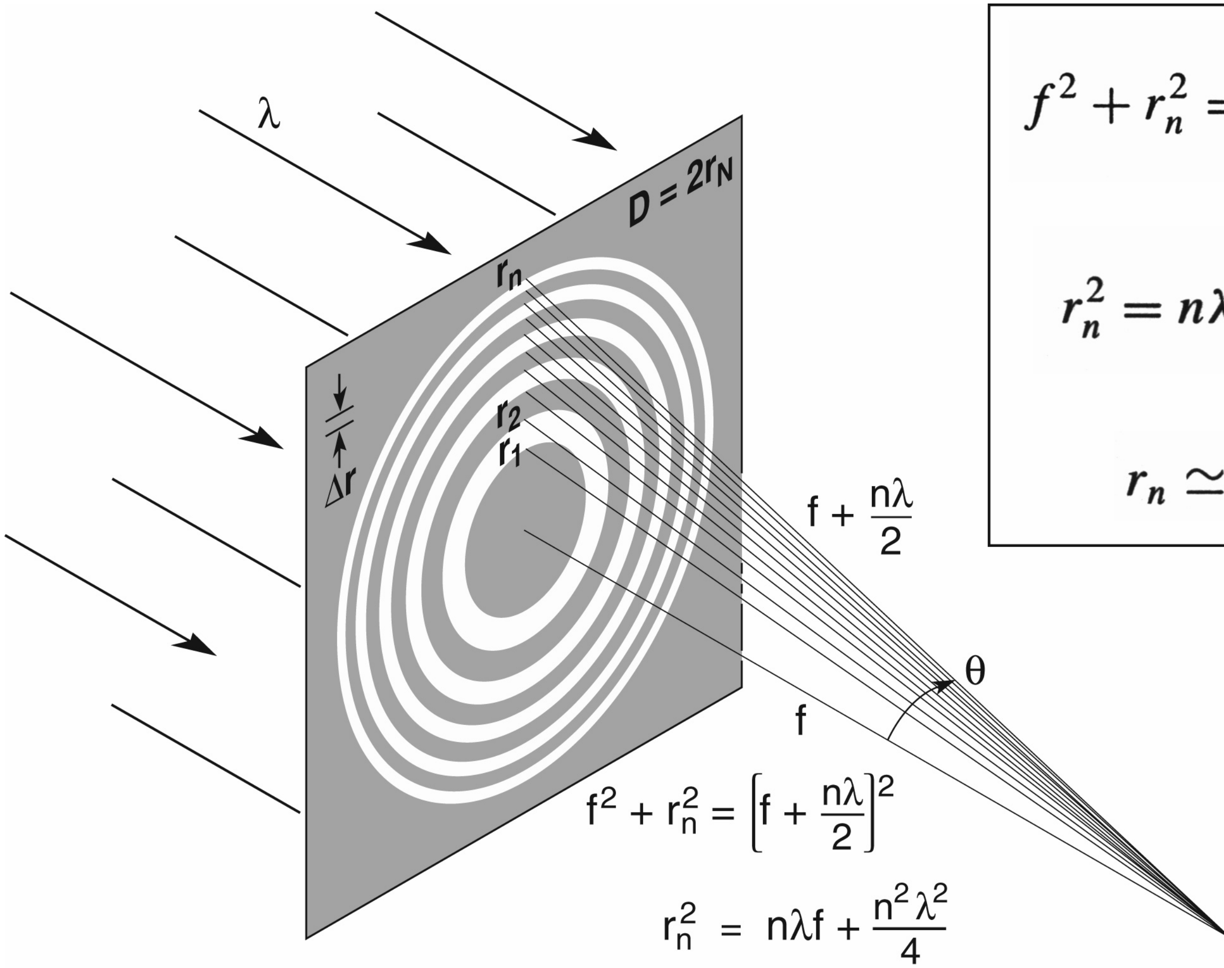

$$f^2 + r_n^2 = \left(f + \frac{n\lambda}{2}\right)^2 \qquad (9.8)$$

$$r_n^2 = n\lambda f + \frac{n^2\lambda^2}{4} \qquad (9.9)$$

$$r_n \simeq \sqrt{n\lambda f} \qquad (9.10)$$

Ch09_F05VG.ai

A Fresnel zone plate lens used as a diffractive lens for point to point imaging

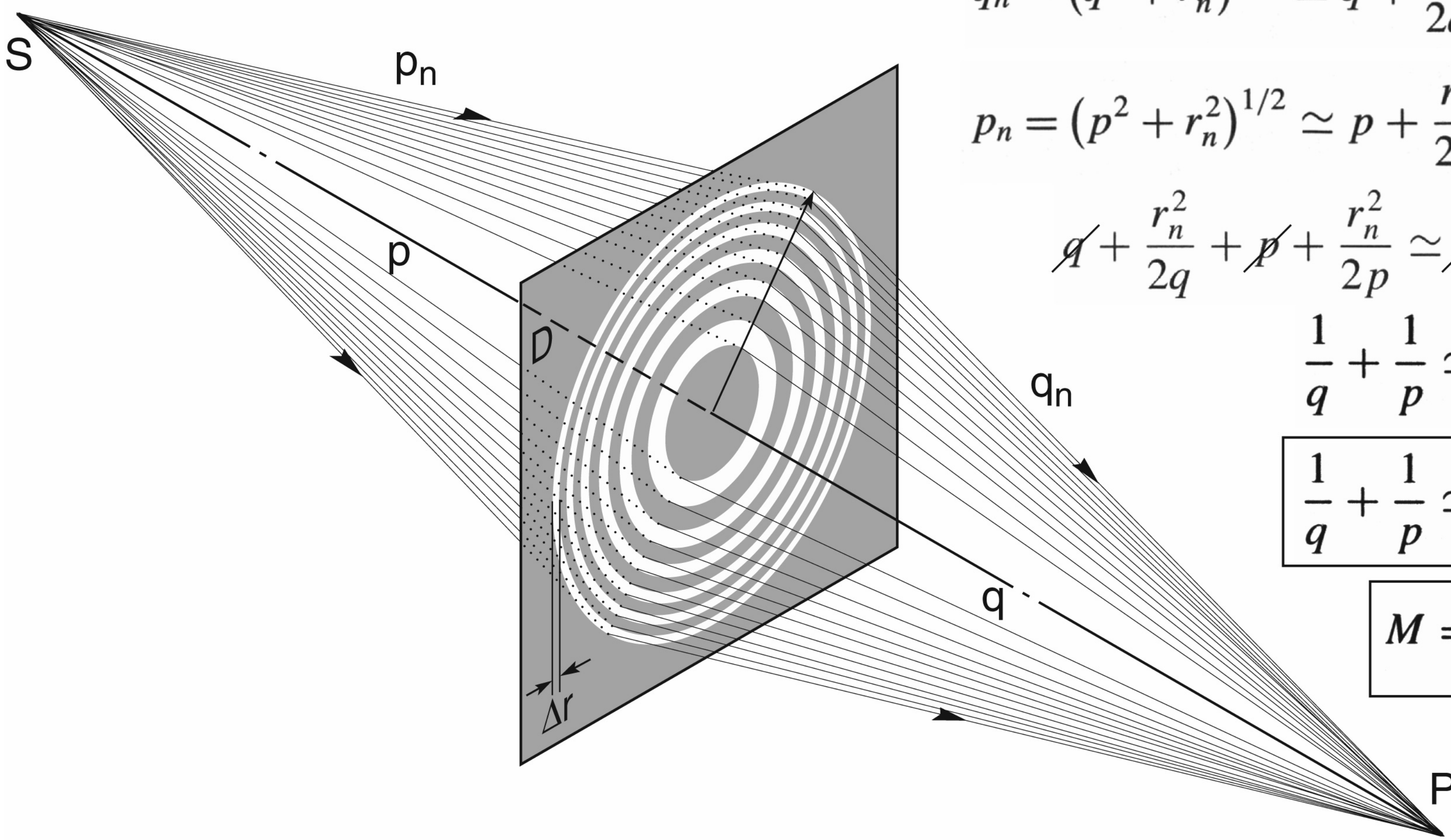

$$q_n + p_n = q + p + \frac{n\lambda}{2}$$

$$q_n = \left(q^2 + r_n^2\right)^{1/2} \simeq q + \frac{r_n^2}{2q}$$

$$p_n = \left(p^2 + r_n^2\right)^{1/2} \simeq p + \frac{r_n^2}{2p}$$

$$\cancel{q} + \frac{r_n^2}{2q} + \cancel{p} + \frac{r_n^2}{2p} \simeq \cancel{q} + \cancel{p} + \frac{n\lambda}{2}$$

$$\frac{1}{q} + \frac{1}{p} \simeq \frac{n\lambda}{r_n^2}$$

$$\boxed{\frac{1}{q} + \frac{1}{p} \simeq \frac{1}{f}} \quad (9.17)$$

$$\boxed{M = \frac{p}{q}} \quad (9.18)$$

Ch09_F02_modif.VG.ai

Depth of focus and spectral bandwidth

$$\Delta z = \pm \frac{1}{2} \frac{\lambda}{(\mathrm{NA})^2} \qquad (9.50)$$

$$\Delta z = \pm 2 F^{\#2} \lambda = \pm 2 (\Delta r)^2 / \lambda \qquad (9.51)$$

$$\frac{\Delta \lambda}{\lambda} \leq \frac{1}{N} \qquad (9.52)$$

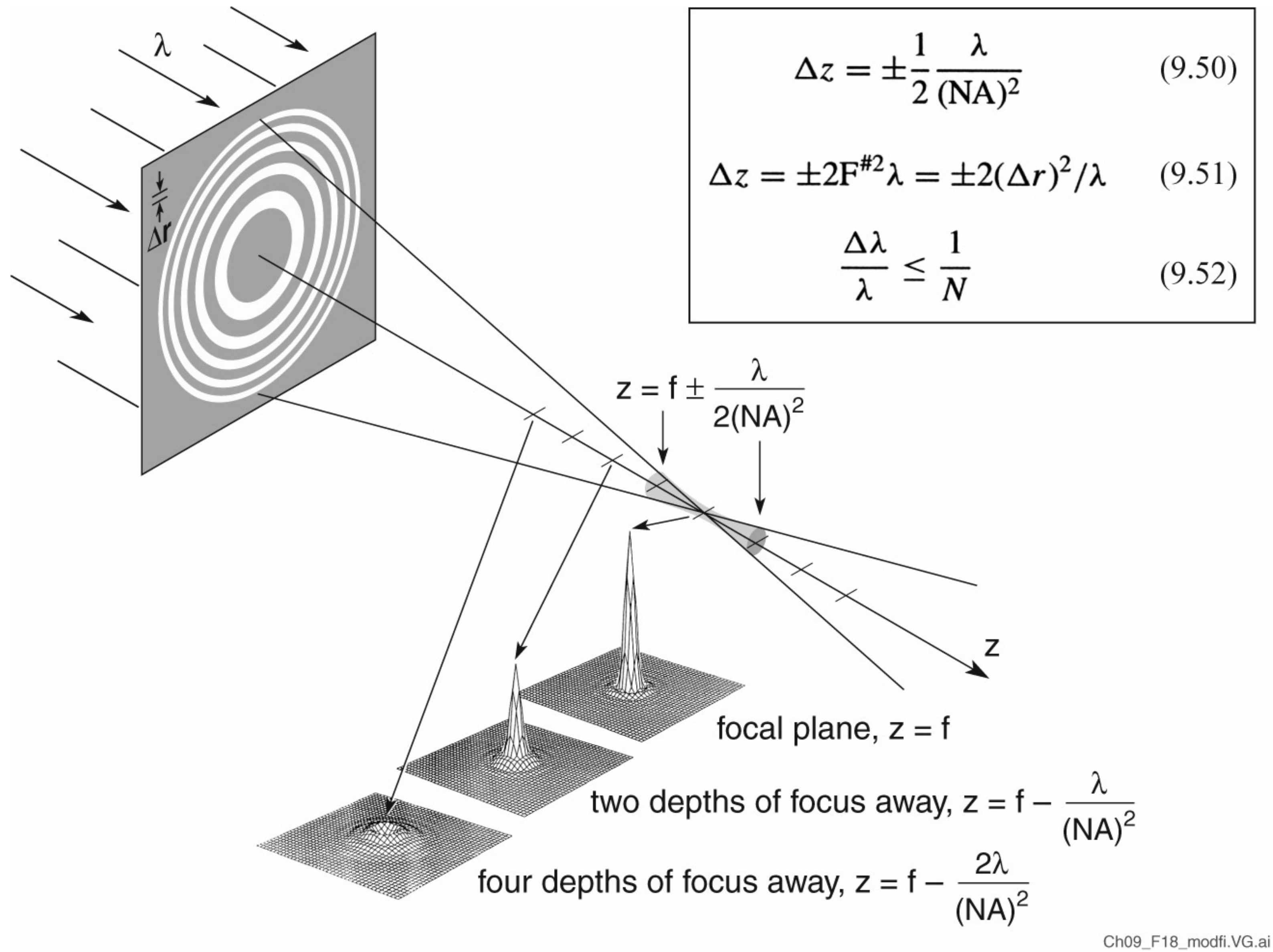

A Fresnel zone plate lens for soft x-ray microscopy

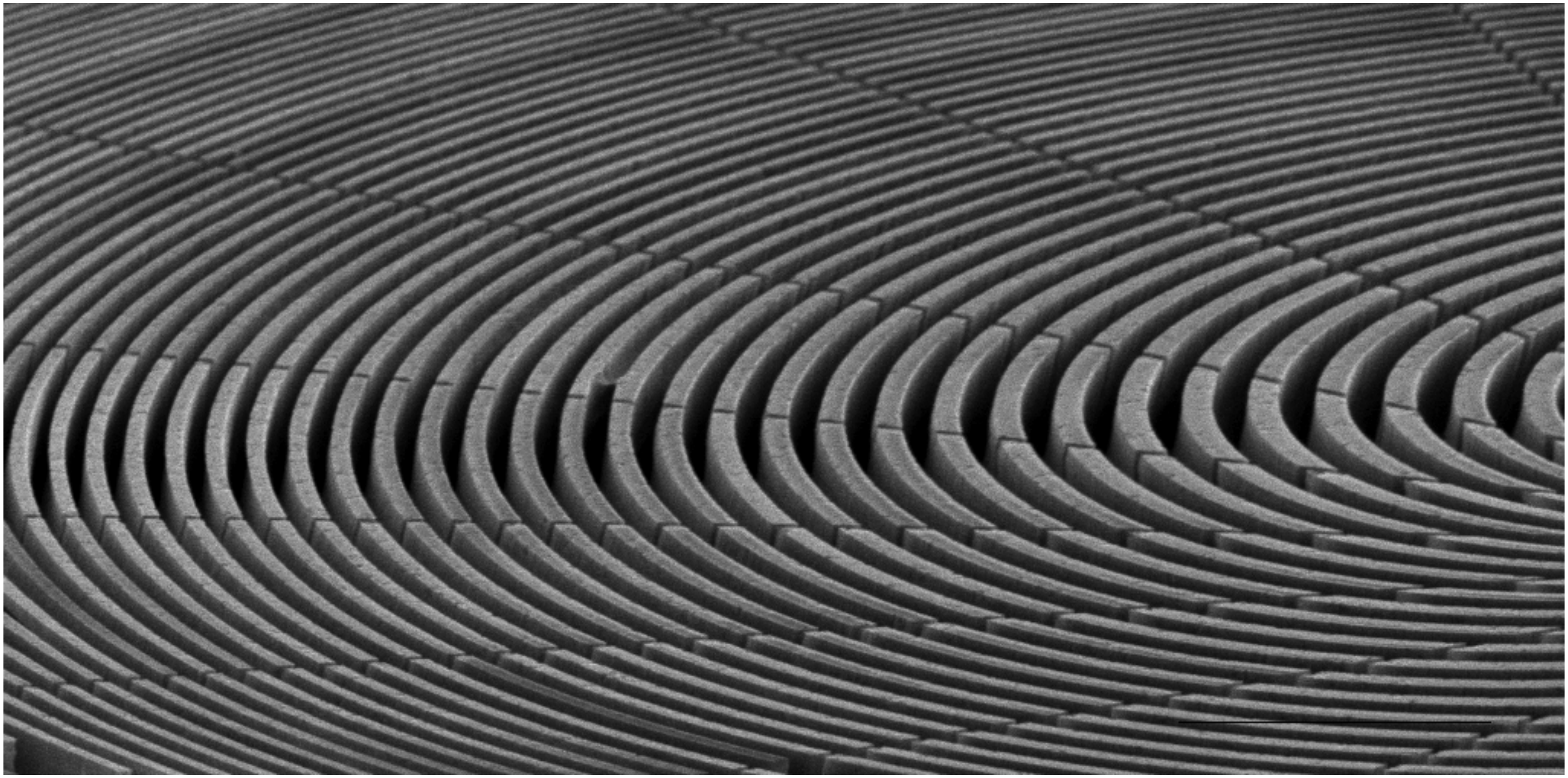

Courtesy of Anne Sakdinawat, SLAC/Stanford; C. Chang and A. Sakdinawat, Nature Communications (27Jun2014).

Dual functionality x-ray lenses: Improving contrast and resolution for x-ray microscopy

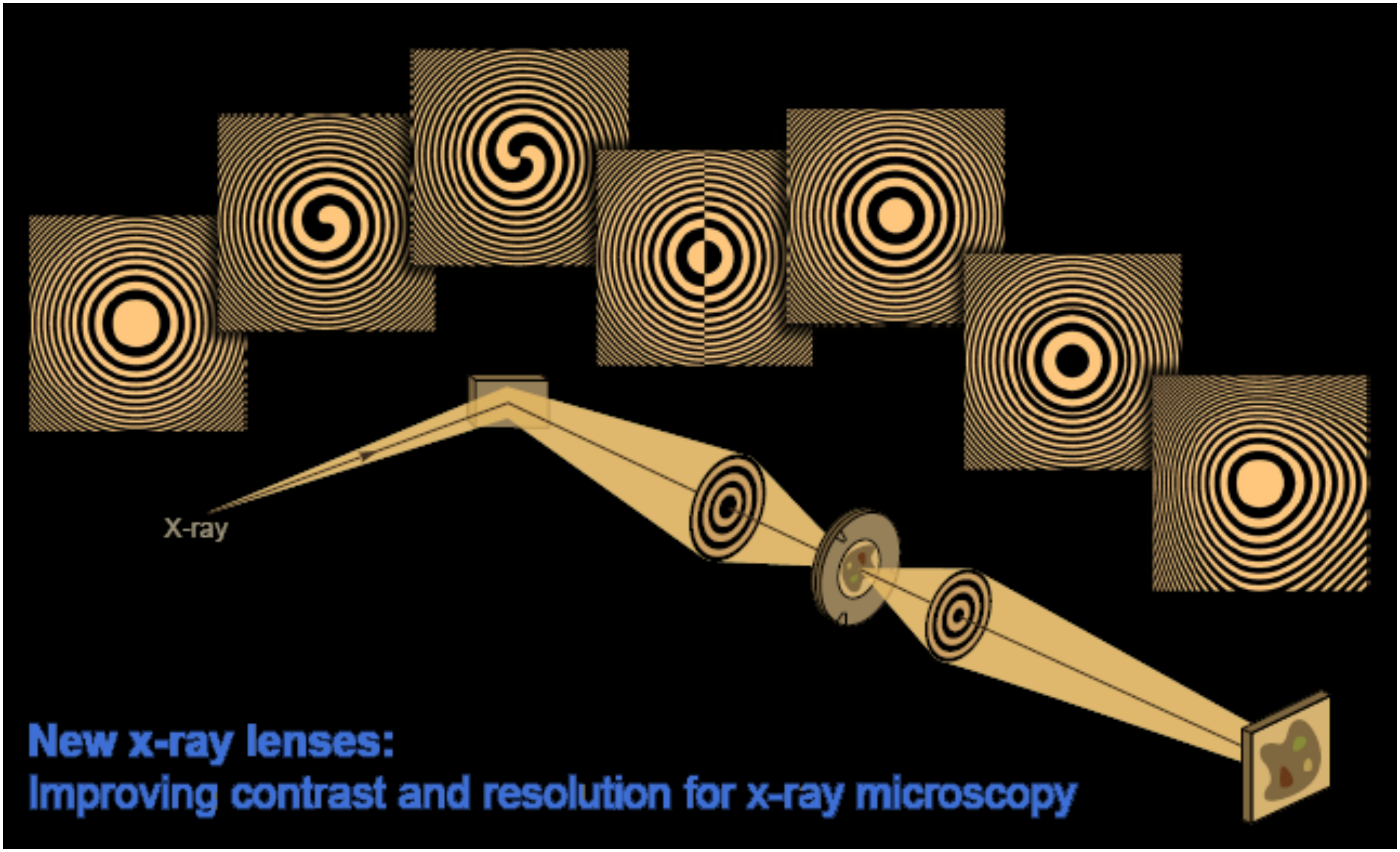

C. Chang, A. Sakdinawat, P.J. Fischer, E.H. Anderson, D.T. Attwood, Opt. Lett. 2006; Sakdinawat and Liu, Opt. Lett. 2007; Sakdinawat and Liu, Opt. Express 2008

New ultra high aspect ratio, high efficiency, hard x-ray zone plates for high spatial resolution at 30-50 keV

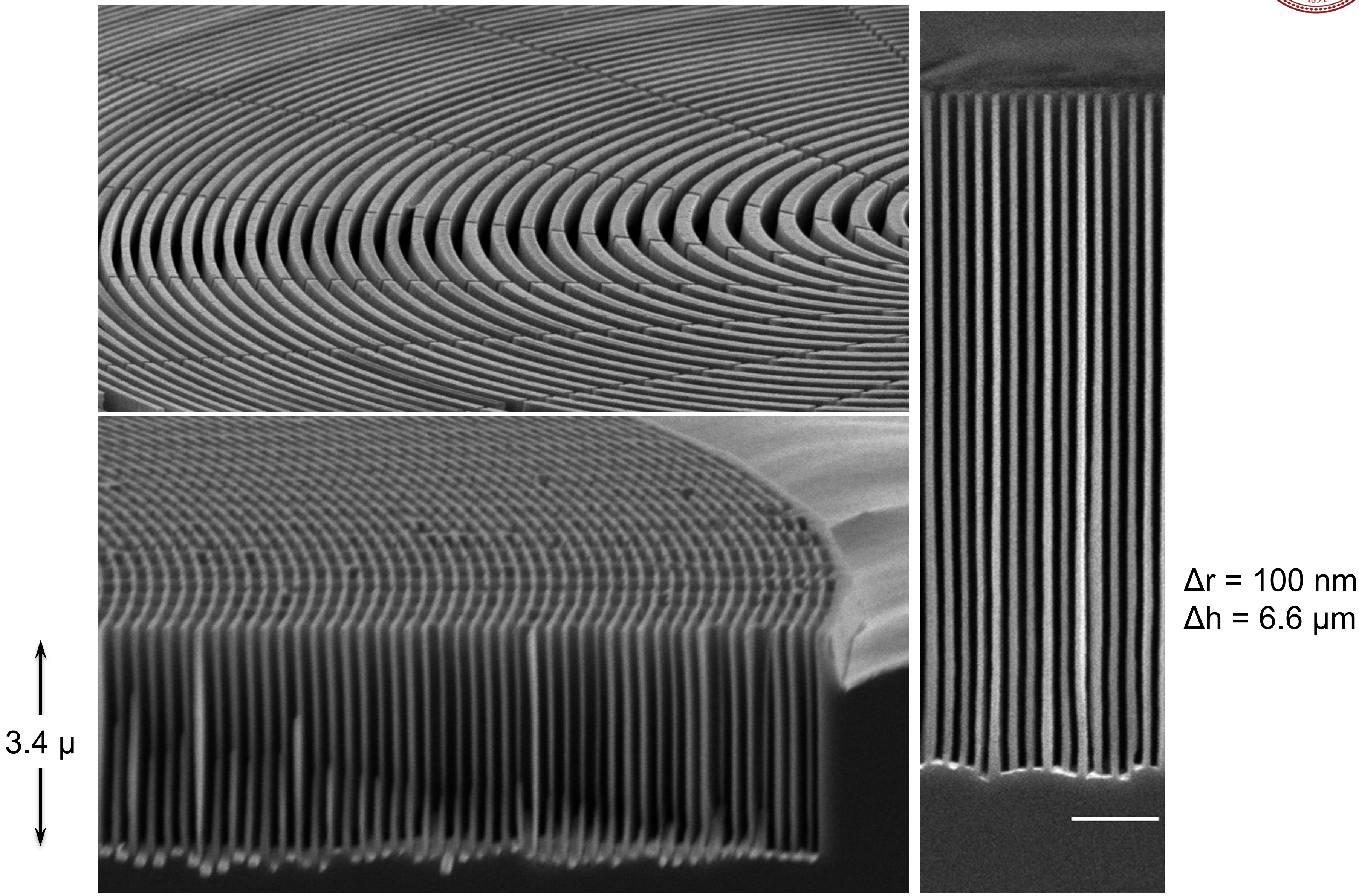

Courtesy of Anne Sakdinawat, SLAC/Stanford; C. Chang and A. Sakdinawat, Nature Communications (27Jun2014).

Diffraction limited x-ray imaging

For example, the widely accepted Rayleigh criteria for resolving two adjacent, mutually incoherent, point sources of light, results in a 26% intensity modulation.

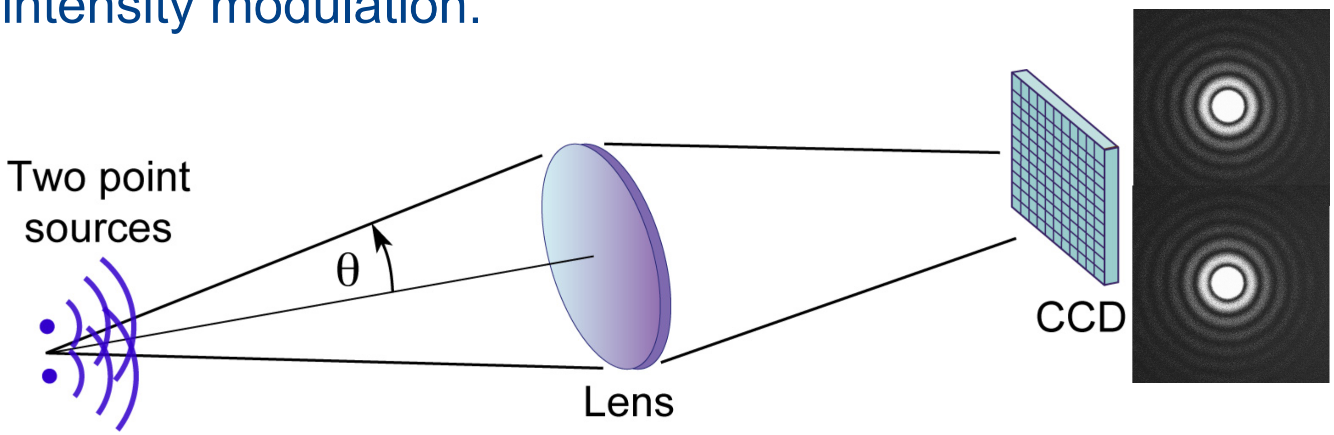

λ = 2.48 nm (500 eV)

Two overlapping Airy patterns

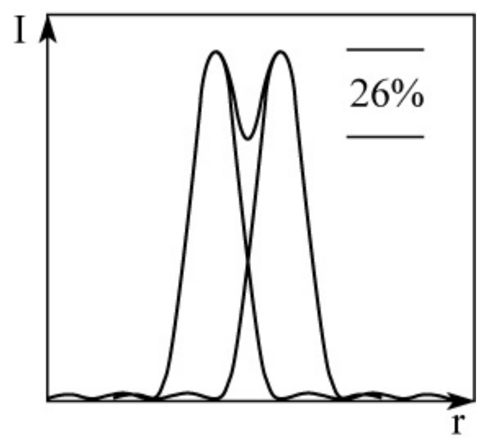

$\Delta r_{resol.} = 0.61\ \lambda / NA$

Resultant intensity pattern when the two point sources are "just resolved", such that the central lobe maximum due to one point source overlaps the first minimum (dark ring) of the other.

Note: Other definitions are possible, depending on the application and the ability to discern separated objects.

Resolution and illumination

Achievable resolution can be improved by varying illumination:

An object pattern of periodicity d diffracts light and is just captured by the lens – setting the diffraction limited resolution limit.

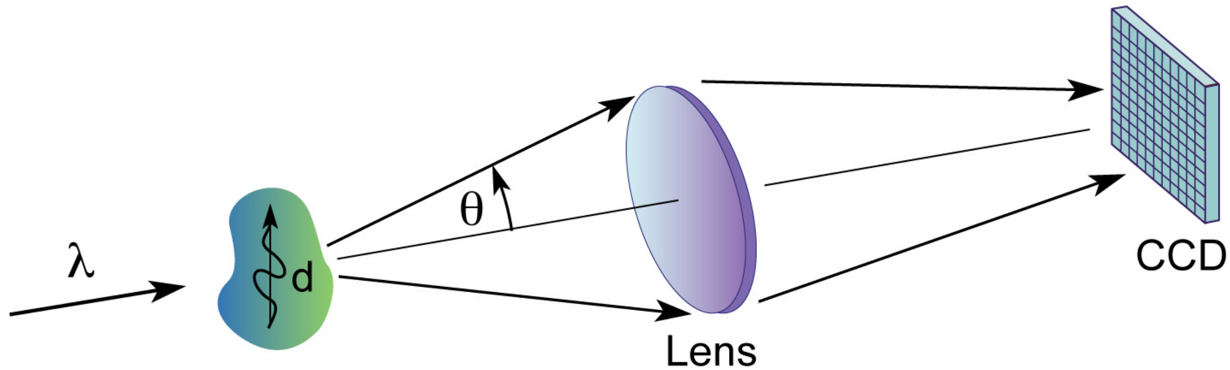

Diffraction from an object of smaller periodicity, d/2, is just captured, and resolved, when illuminated from an angle.

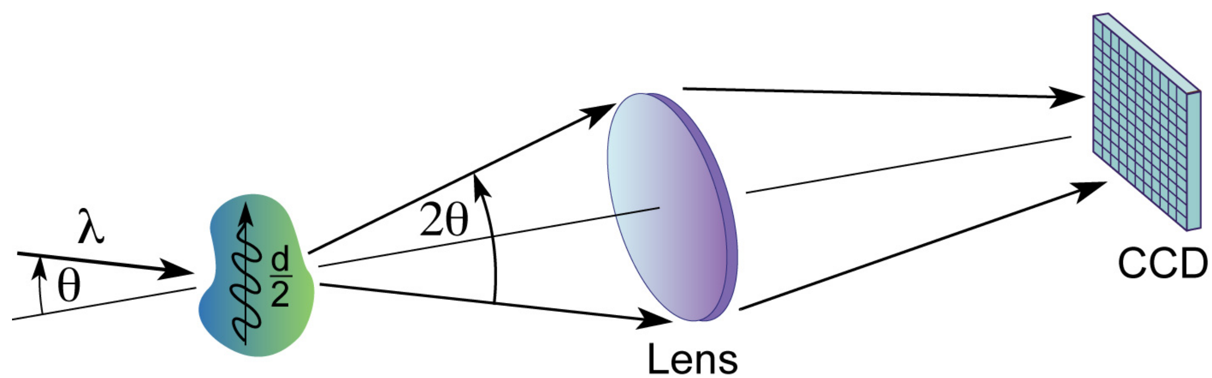

Resolution, illumination, and optical transfer function

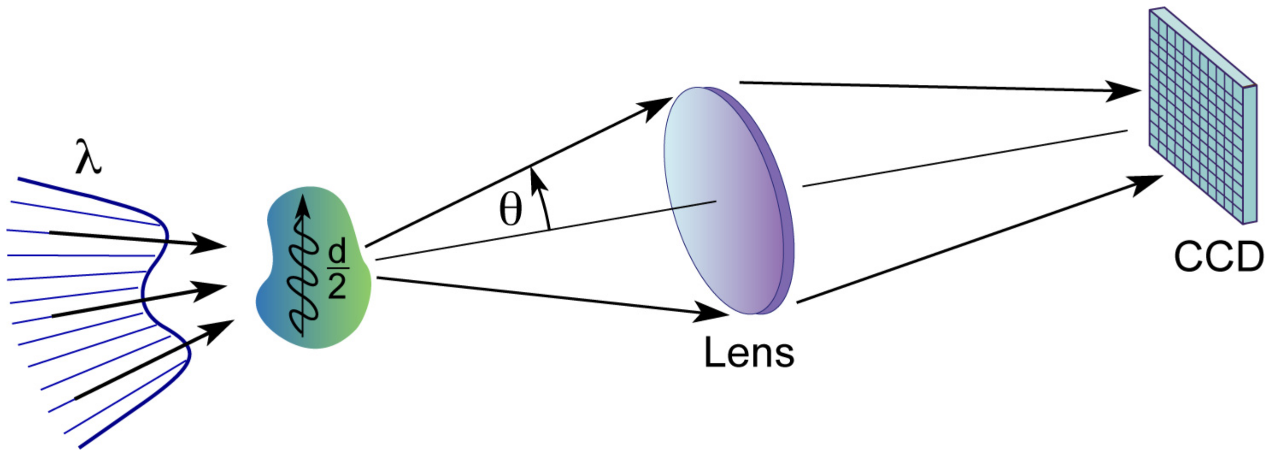

Spatial frequency response of the optical system can be optimized by tailoring the angular distribution of illumination.

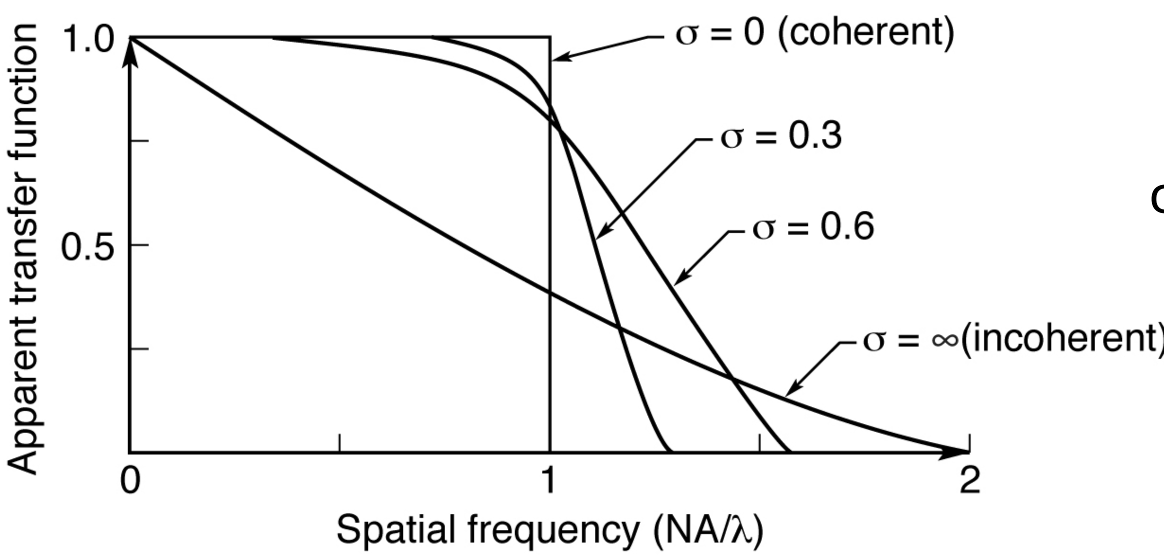

$$\sigma = \frac{NA_{cond}}{NA_{obj}} \qquad (10.3)$$

Nature Vol 435|30 June 2005|doi:10.1038/nature-3719

LETTERS

Soft X-ray microscopy at a spatial resolution better than 15 nm

Weilun Chao[1,2], Bruce D. Harteneck[1], J. Alexander Liddle[1], Erik H. Anderson[1] & David T. Attwood[1,2]

Analytical tools that have spatial resolution at the nanometre scale are indispensable for the life and physical sciences. It is desirable that these tools also permit elemental and chemical identification on a scale of 10 nm or less, with large penetration depths. A variety of techniques[1–7] in X-ray imaging are currently being developed that may provide these combined capabilities. Here we report the achievement of sub-15-nm spatial resolution with a soft X-ray microscope—and a clear path to below 10 nm—using an overlay technique for zone plate fabrication. The microscope covers a spectral range from a photon energy of 250 eV (~5 nm wavelength) to 1.8 keV (~0.7 nm), so that primary K and L atomic resonances of elements such as C, N, O, Al, Ti, Fe, Co and Ni can be probed. This X-ray microscopy technique is therefore suitable for a wide range of studies: biological imaging in the water window[8,9]; studies of wet environmental samples[10,11]; studies of magnetic nanostructures with both elemental and spin-orbit sensitivity[12–14]; studies that require viewing through thin windows, coatings or substrates (such as buried electronic devices in a silicon chip[15]); and three-dimensional imaging of cryogenically fixed biological cells[9,16].

The microscope XM-1 at the Advanced Light Source (ALS) in Berkeley[17] is schematically shown in Fig. 1. The microscope type is similar to that pioneered by the Göttingen/BESSY group (ref. 18, and references therein). A 'micro' zone plate (MZP) projects a full-field image to an X-ray-sensitive CCD (charge-coupled device), typically in one or a few seconds, often with several hundred images per day. The field of view is typically 10 μm, corresponding to a magnification of 2,500. The condenser zone plate (CZP), with a central stop, serves two purposes in that it provides partially coherent hollow-cone illumination[2], and, in combination with a pinhole, serves as the monochromator. Monochromatic radiation of $\lambda/\Delta\lambda = 500$ is used. Both zone plates are fabricated in-house, using electron beam lithography[19].

The spatial resolution of a zone plate based microscope is equal to $k_1\lambda/\mathrm{NA}_{MZP}$, where λ is the wavelength, NA_{MZP} is the numerical aperture of the MZP, and k_1 is an illumination dependent constant, which ranges from 0.3 to 0.61. For a zone plate lens used at high magnification, $\mathrm{NA}_{MZP} = \lambda/2\Delta r_{MZP}$, where Δr_{MZP} is the outermost (smallest) zone width of the MZP[20]. For the partially coherent illumination[21,22] used here, $k_1 \approx 0.4$ and thus the theoretical resolution is $0.8\Delta_{MZP}$, as calculated using the SPLAT computer program[23] (a two-dimensional scalar diffraction code, which evaluates partially coherent imaging). In previous results with a $\Delta r_{MZP} = 25$ nm zone plate, we reported[2] an unambiguous spatial resolution of 20 nm. Here we describe the use of an overlay nanofabrication technique that allows us to fabricate zone plates with finer outer zone widths, to $\Delta r_{MZP} = 15$ nm, and to achieve a spatial resolution of below 15 nm, with clear potential for further extension.

This technique overcomes nanofabrication limits due to electron beam broadening in high feature density patterning. Beam broadening results from electron scattering within the recording medium (resist), leading to a loss of image contrast and thus resolvability for

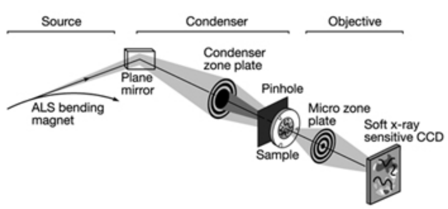

Figure 1 | A diagram of the soft X-ray microscope XM-1. The microscope uses a micro zone plate to project a full field image onto a CCD camera that is sensitive to soft X-rays. Partially coherent, hollow-cone illumination of the sample is provided by a condenser zone plate. A central stop and a pinhole provide monochromatization.

[1]Center for X-ray Optics, Lawrence Berkeley National Laboratory, 1 Cyclotron Road, MS 2-400, [2]Department of Electrical Engineerin California, Berkeley, California 94720, USA.

$\lambda = 1.52$ nm (815 eV)

$\Delta r = 15$ nm

$N = 500$

$D = 30$ μm

$f = 300$ μm

$\sigma = 0.38$

$0.8\,\Delta r = 12$ nm

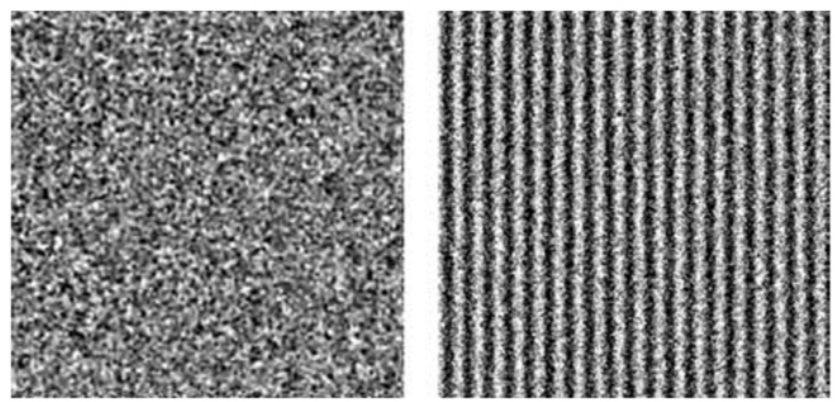

Figure 4 | Soft X-ray images of a 15.1 nm half-period test object, as formed with zone plates having outer zone widths of 25 nm and 15 nm.

Cr/Si test pattern (Cr L_3 @ 574 eV)
(2000 X 2000, 10^4 ph/pixel)

Hard x-ray zone plate microscopy

- Shorter wavelengths, potentially better spatial resolution and greater depth-of-field.
- Less absorption (β); phase shift (δ) dominates, higher efficiency.
- Thicker structures required (e.g., zones), higher aspect ratios pose nanofabrication challenges.
- Contrast of nanoscale samples minimal; will require good statistics, uniform background, dose mitigation.

A high quality Mo/Si multilayer mirror

N = 40
d = 6.7

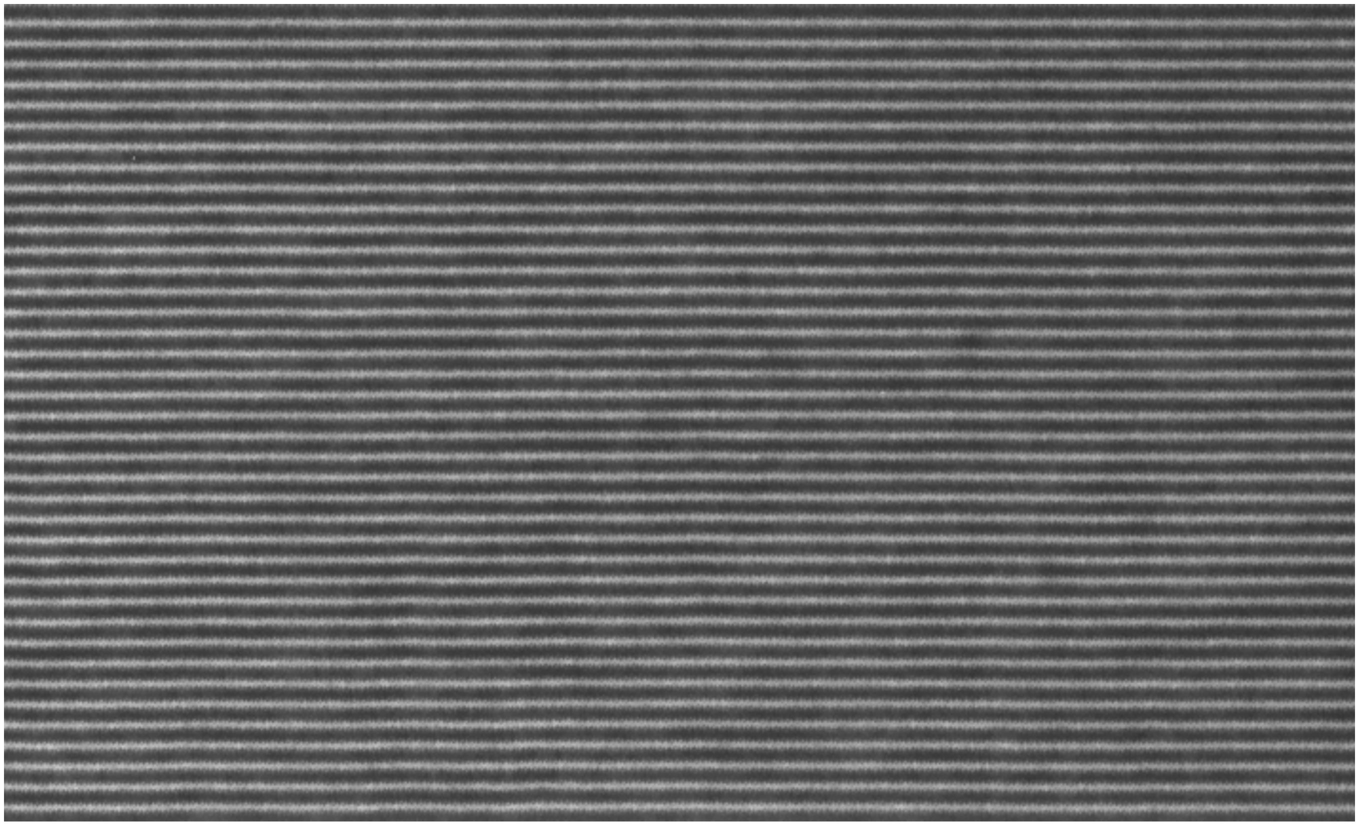

Courtesy of Saša Bajt (LLNL, now DESY)

Scattering by density variations within a multilayer coating

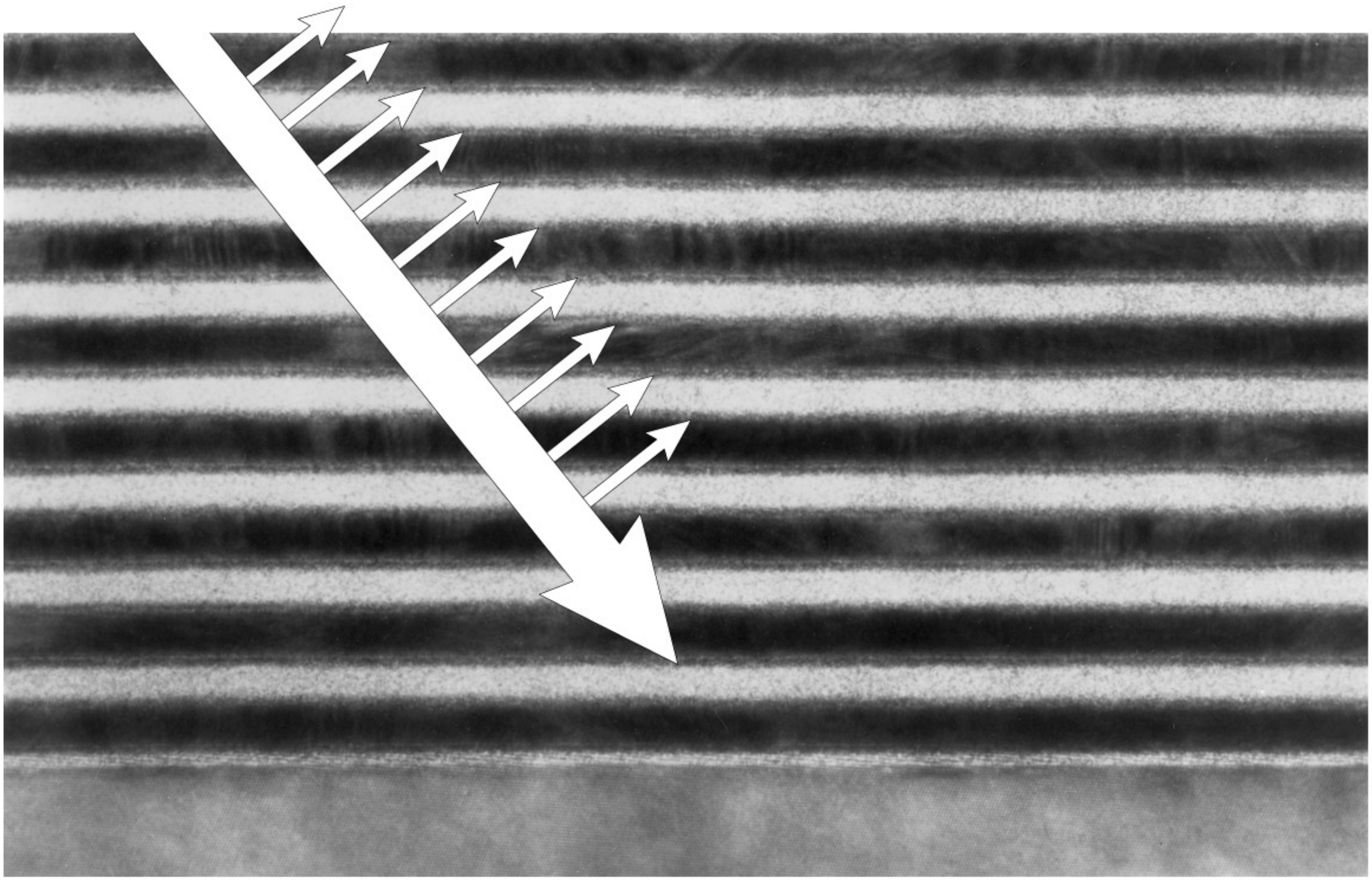

(T. Nguyen, CXRO/LBNL)

Ch04_F01_Feb2007.ai

Multilayer mirrors satisfy the Bragg condition

$$m\lambda = 2d \sin\theta$$

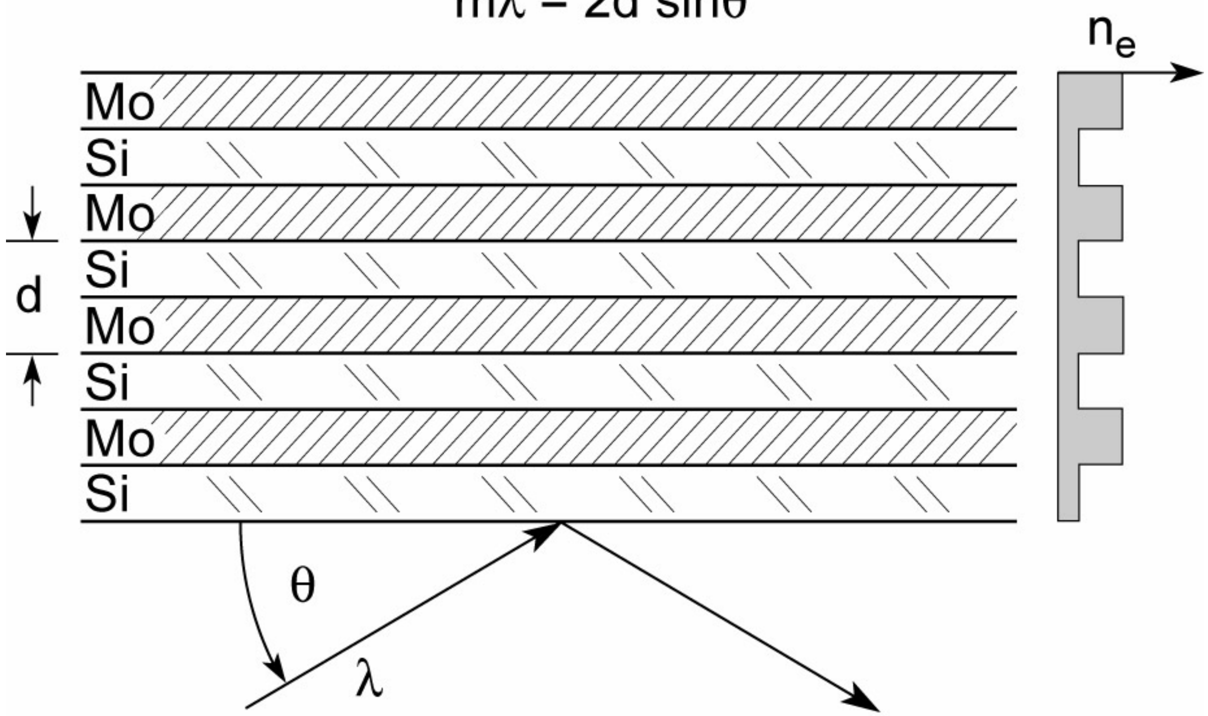

For normal incidence, $\theta = \pi/2$, first order ($m = 1$) reflection

$$\lambda = 2d$$

$$d = \lambda/2$$

if the two layers are approximately equal

$$\Delta t \simeq \lambda/4$$

a quarter-wave plate coating.

Ch04_MltlyrMirBragg1.ai

High reflectivity, thermally and environmentally robust multilayer coatings for high throughput EUV lithography

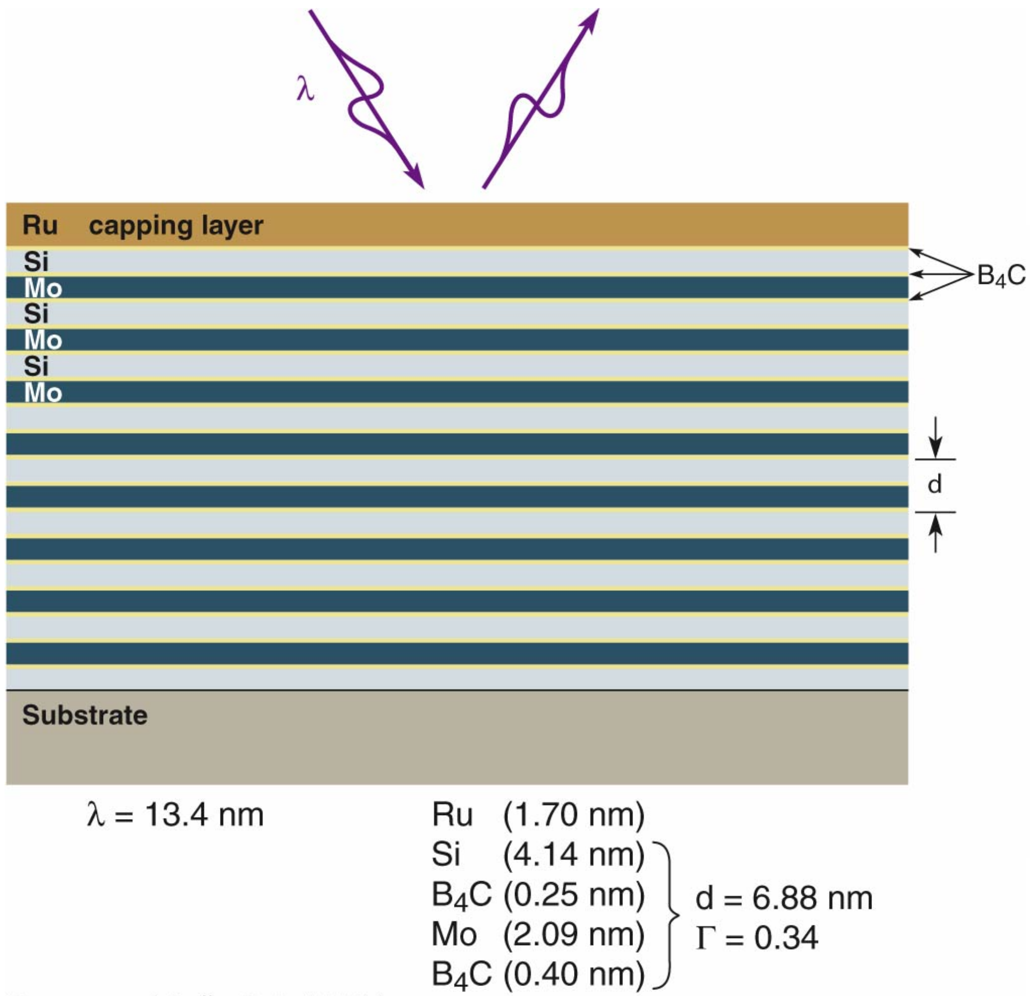

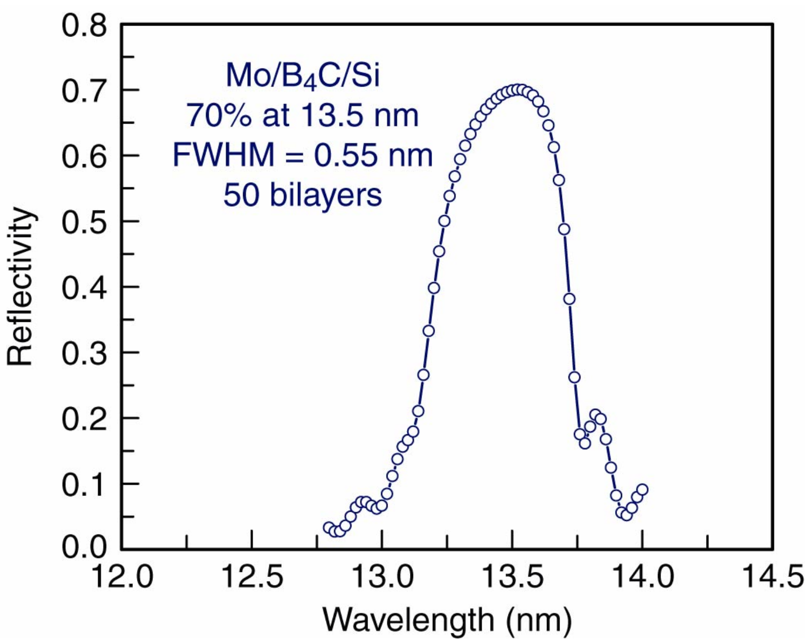

Courtesy of Saša Bajt (LLNL)

Atomic scattering factors for silicon (Z = 14)

σ_a(barns/atom) = μ(cm^2/g) × 46.64
E(keV)μ(cm^2/g) = f_2^0 × 1498.22

Silicon (Si)
Z = 14
Atomic weight = 28.086

Energy (eV)	f_1^0	f_2^0	μ(cm^2/g)
30	3.799	3.734E–01	1.865E+04
70	2.448	5.701E–01	1.220E+04
100	–5.657	4.580E+00	6.862E+04
300	12.00	6.439E+00	3.216E+04
700	13.31	1.951E+00	4.175E+03
1000	13.00	1.070E+00	1.602E+03
3000	14.23	1.961E+00	9.792E+02
7000	14.33	4.240E–01	9.075E+01
10000	14.28	2.135E–01	3.199E+01
30000	14.02	2.285E–02	1.141E+00

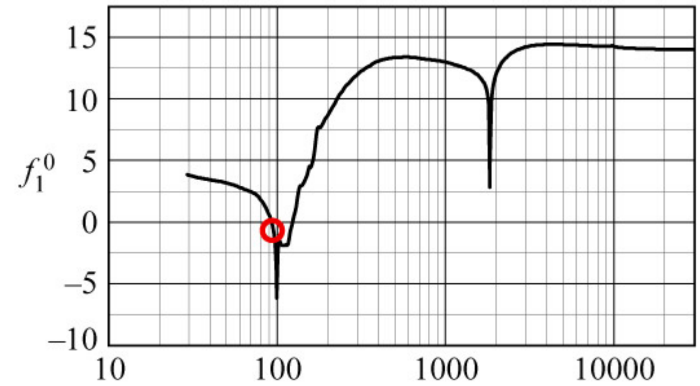

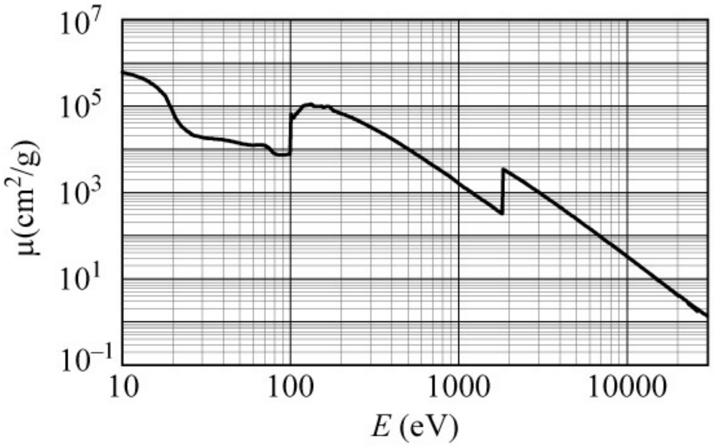

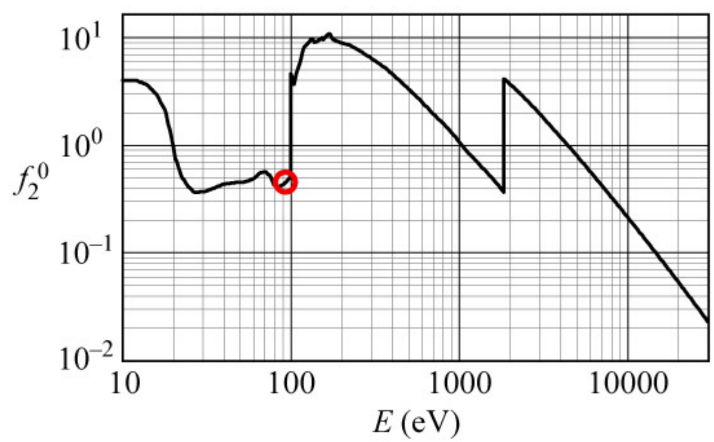

Edge Energies: K 1838.9 eV L_1 149.7 eV
L_2 99.8 eV
L_3 99.2 eV

(Henke and Gullikson; www-cxro.LBL.gov)

Ch02ApC_Tb1F07_Sept05.ai

Atomic scattering factors for molybdenum (Z = 42)

$\sigma_a(\text{barns/atom}) = \mu(\text{cm}^2/\text{g}) \times 159.31$

$E(\text{keV})\mu(\text{cm}^2/\text{g}) = f_2^0 \times 438.59$

Molybdenum (Mo)
Z = 42
Atomic weight = 95.940

Energy (eV)	f_1^0	f_2^0	$\mu(\text{cm}^2/\text{g})$
30	1.071	5.292E+00	7.736E+04
70	19.38	4.732E+00	2.965E+04
100	14.02	1.124E+00	4.931E+03
300	4.609	1.568E+01	2.292E+04
700	31.41	1.819E+01	1.140E+04
1000	35.15	1.188E+01	5.210E+03
3000	35.88	1.366E+01	1.997E+03
7000	42.11	3.493E+00	2.189E+02
10000	41.67	1.881E+00	8.248E+01
30000	42.04	1.894E+00	2.769E+01

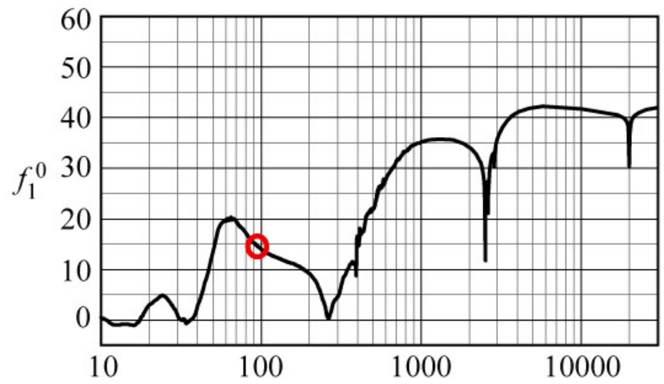

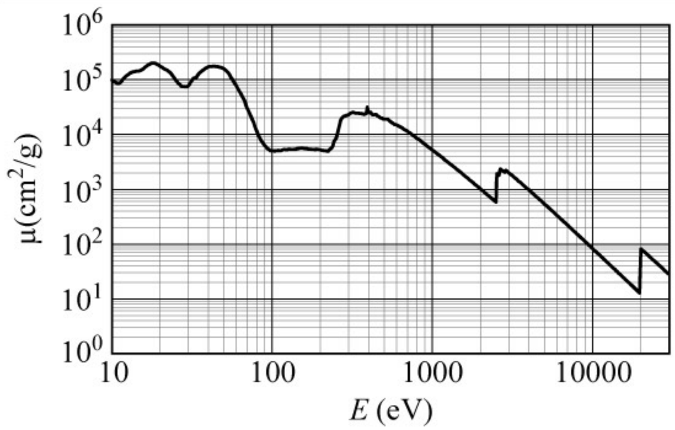

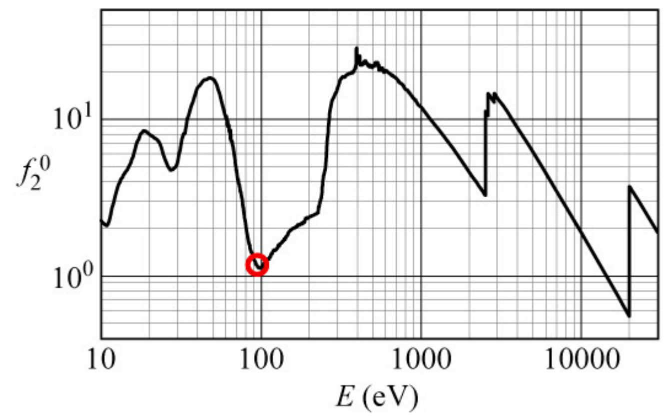

Edge Energies:

K	19999.5 eV	L_1	2865.5 eV	M_1	506.3 eV	N_1	63.2 eV
		L_2	2625.1 eV	M_2	411.6 eV	N_2	37.6 eV
		L_3	2520.2 eV	M_3	394.0 eV	N_3	35.5 eV
				M_4	231.1 eV		
				M_5	227.9 eV		

(Henke and Gullikson; www-cxro.LBL.gov)

Ch02ApC_Tb1F12_June2008.ai

Sputtered deposition of a multilayer coating

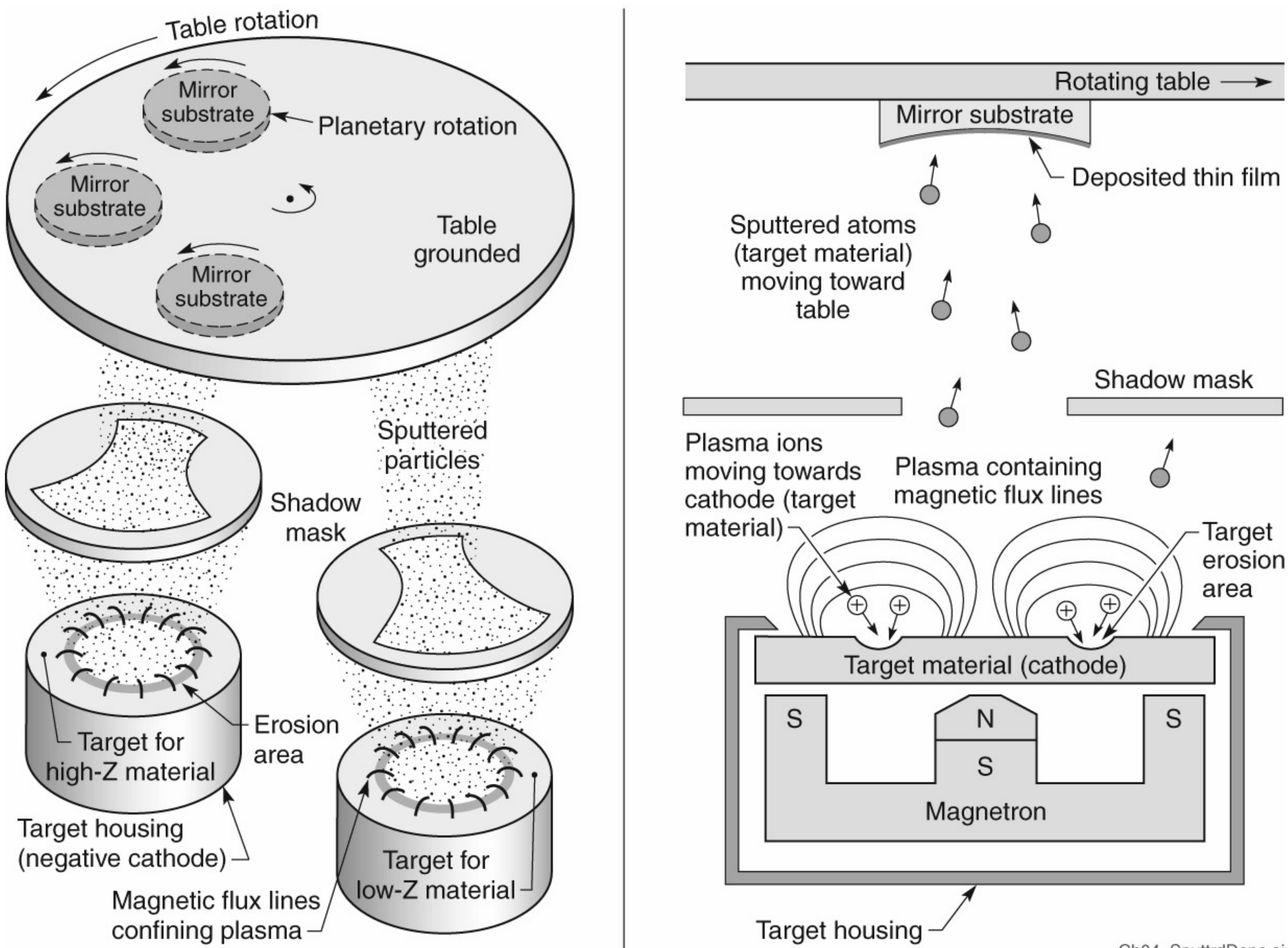

Time structure of synchrotron radiation

The axial electric field within the RF cavity, used to replenish lost (radiated) energy, forms a potential well "bucket" system that forces electrons into axial electron "bunches". This leads to a time structure in the emitted radiation.

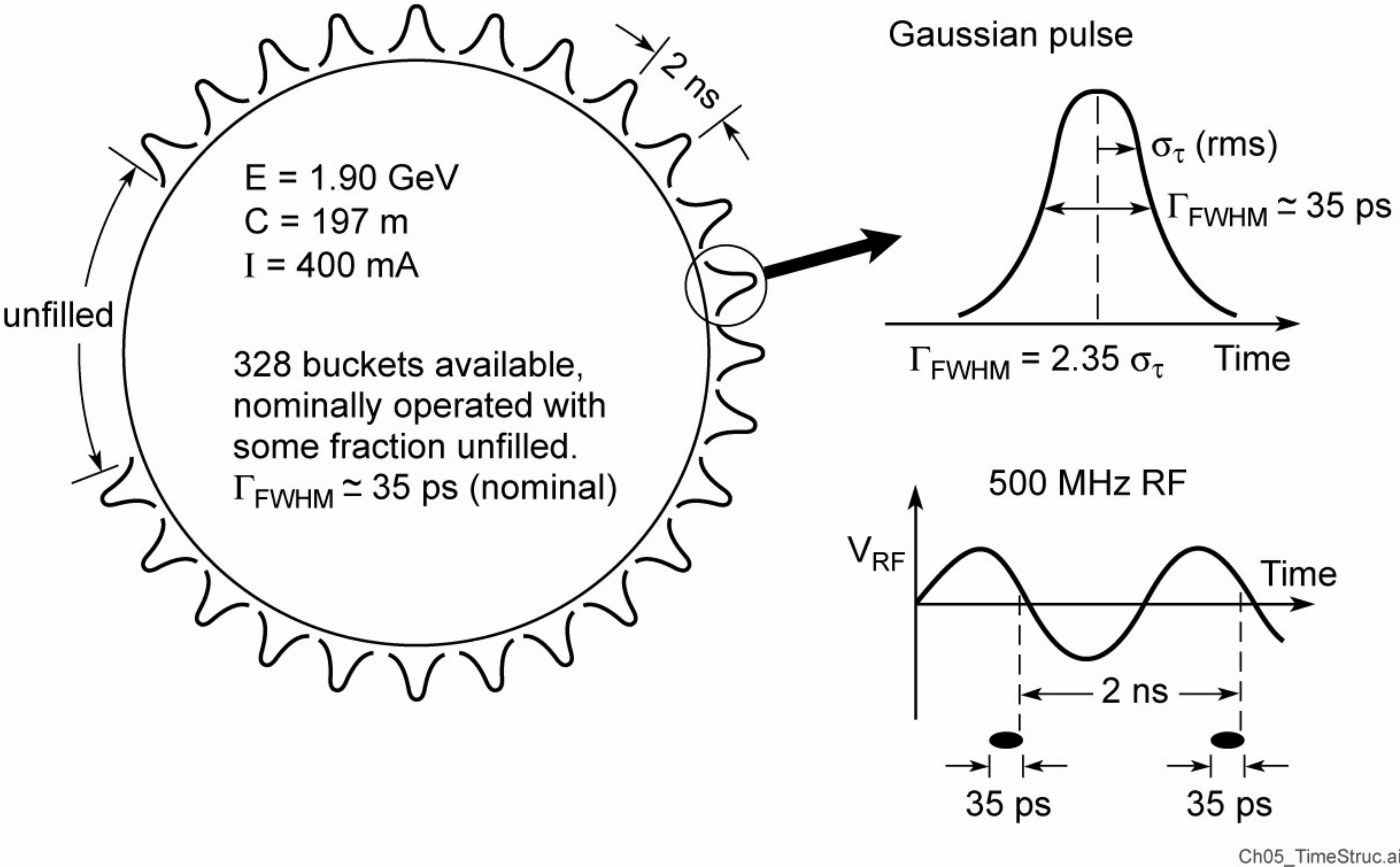

Typical parameters for synchrotron radiation

Facility	ALS	New Subaru	APS	SP-8
Electron energy	1.90 GeV	1.00 GeV	7.00 GeV	8.00 GeV
γ	3720	1957	13,700	15,700
Current (mA)	400	100	100	100
Circumference (m)	197	119	1100	1440
RF frequency (MHz)	500	500	352	509
Pulse duration (FWHM) (ps)	35-70	26	100	120
Bending Magnet Radiation:				
Bending magnet field (T)	1.27	1.03	0.599	0.679
Critical photon energy (keV)	3.05	0.685	19.5	28.9
Critical photon wavelength	0.407 nm	1.81 nm	0.636 Å	0.429 Å
Bending magnet sources	24	4	35	23
Undulator Radiation:				
Number of straight sections	12	4	40	48
Undulator period (typical) (cm)	5.00	5.40	3.30	3.20
Number of periods	89	200	72	140
Photon energy ($K = 1, n = 1$)	457 eV	117 eV	9.40 keV	12.7 keV
Photon wavelength ($K = 1, n = 1$)	2.71 nm	10.6 nm	1.32 Å	0.979 Å
Tuning range ($n = 1$)	230-620 eV	43-170 eV	3.5-12 keV	4.7-19 keV
Tuning range ($n = 3$)	690-1800 eV	130-500 eV	10-38 keV	16-51 keV
Central cone half-angle ($K = 1$)	35 μrad	44 μrad	11 μrad	6.6 μrad
Power in central cone ($K = 1, n = 1$) (W)	2.3	0.15	12	16
Flux in central cone (photons/s)	3.1×10^{16}	7.9×10^{15}	7.9×10^{15}	7.9×10^{15}
σ_x, σ_y (μm)	260, 16	450, 220	320, 50	380, 6.8
σ'_x, σ'_y (μrad)	23, 3.9	89, 18	23, 7	16, 1.8
Brightness ($K = 1, n = 1$)[a] [(photons/s)/mm^2 · mrad^2 · (0.1%BW)]	2.3×10^{19}	1.7×10^{17}	5.9×10^{18}	1.8×10^{20}
Total power ($K = 1$, all n, all θ) (W)	83	27	350	2,000
Other undulator periods (cm)	3.65, 8.00, 10.0	7.60	2.70, 5.50, 12.8	2.4, 10.0, 3.7, 12.0
Wiggler Radiation:				
Wiggler period (typical) (cm)	16.0		8.5	12.0
Number of periods	19		28	37
Magnetic field (maximum) (T)	2.1		1.0	1.0
K (maximum)	32		7.9	11
Critical photon energy (keV)	5.1		33	43
Critical photon wavelength	0.24 nm		0.38 Å	0.29 Å
Total power (max. K) (kW)	13		7.4	18

[a] Using Eq. (5.65). See comments following Eq. (5.64) for the case where $\sigma'_{x,y} \simeq \theta_{cen}$.

Ch05_T1b_VG_Nov05.ai

Photon energy, wavelength, power

$$\hbar\omega \cdot \lambda = hc = 1239.842 \text{ eV nm} \qquad (1.1)$$

$$1 \text{ joule} \Rightarrow 5.034 \times 10^{15} \lambda[\text{nm}] \text{ photons} \qquad (1.2a)$$

$$1 \text{ watt} \Rightarrow 5.034 \times 10^{15} \lambda[\text{nm}] \, \frac{\text{photons}}{\text{s}} \qquad (1.2b)$$

Ch01_Eqs1.1_2.ai

CXRO Web Site

X-Ray Interactions with Matter . Search CXRO

Facilities

Publications

Research

X-Ray Tools

Visitors

Personnel

Comments?

Server Stats

www.cxro.LBL.gov/

- **Atomic scattering factors**
- **EUV/x-ray properties of the elements**
- **Index of refraction for compound materials**
- **Absorption, attenuation lengths, transmission**
- **EUV/x-ray reflectivity (mirrors, thin films, multilayers)**
- **Transmission grating efficiencies**
- **Multilayer mirror achievements**
- **Other**

2nd Edition in progress: new FEL, HHG, Coherence, and X-ray Imaging chapters

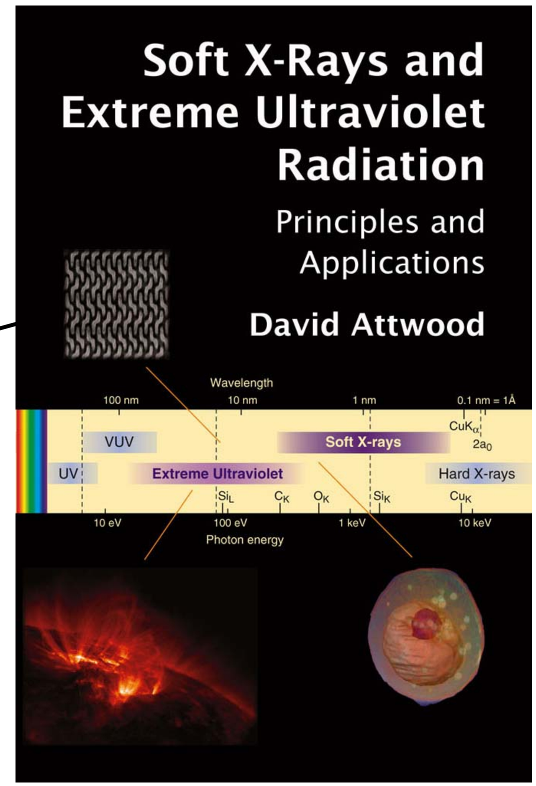

UC Berkeley
www.coe.AST.berkeley.edu/sxr2009
www.coe.AST.berkeley.edu/srms
www.youtube.com